Hindawi
International Transactions on Electrical Energy Systems
Volume 2023, Article ID 6679740, 24 pages
https://doi.org/10.1155/2023/6679740

Research Article

Comparative Analysis of Energy Storage Technologies for Microgrids

Mohamed Haikel Chehab,[1] **Chokri Ben Salah**,[1,2] **Ruben Zieba Falama**,[3] **Mehdi Tlija**,[4] **and Abdelhamid Rabhi**[5]

[1]*Laboratory of Automation, Electrical Systems and Environment (LASEE), University of Monastir, Monastir, Tunisia*
[2]*Issat Sousse, University of Sousse, Sousse, Tunisia*
[3]*National Advanced School of Mines and Petroleum Industries, University of Maroua, P.O. Box 46, Maroua, Cameroon*
[4]*Department of Industrial Engineering, College of Engineering, King Saud University, P.O. Box 800, Riyadh 11421, Saudi Arabia*
[5]*MIS Laboratory, University of Picardie Jules Verne, Amiens 80000, France*

Correspondence should be addressed to Ruben Zieba Falama; rubenziebafalama@gmail.com

Received 3 April 2023; Revised 2 October 2023; Accepted 24 November 2023; Published 12 December 2023

Academic Editor: C. Dhanamjayulu

Nowadays, microgrids (MGs) are receiving a lot of attention. In an economical MG, the battery energy storage system (BESS) plays an important role. One of the biggest challenges in MGs is the optimal choice of the BESS that can lead to better performance of the MG, which will be more flexible, efficient, and effective than traditional power systems. In this paper, we present the modeling and simulation of different energy storage systems including Li-ion, lead-acid, nickel cadmium (Ni-Cd), nickel-metal hybrid (Ni-Mh), and supercapacitor (SC), for renewable energy applications, and more specifically for MGs. The results of simulation show that Li-ion batteries have a better response time than lead-acid batteries, Ni-Cd batteries, and Ni-Mh batteries and thus are more suitable for combination with supercapacitors. Li-ion batteries are the best option for fast-charging applications in MGs. The discharge phase ends with SOC ≤ ±94%, SOC ≤ ±95%, SOC = 95%, SOC < 95%, and SOC < 60%, respectively, for Li-ion, lead-acid, Ni-Cd, Ni-Mh, and supercapacitor. Moreover, the use of the battery management system (BMS) can significantly improve the performance of BESS, leading to higher levels of SOC and longer life span. The obtained results have shown that with an optimization algorithm for energy storage systems, more specifically for the battery-charging mode, the response time of BESSs can be further improved. The effect of ambient temperature has also been investigated on the functional capacities of the batteries. The obtained results demonstrated that extreme temperatures (80°C to −80°C) have a significant impact on battery performance and capacity, especially for Li-ion batteries, with a drop in capacity of up to 50% at −40°C. This highlights the importance of considering the ambient temperature in the design and operation of MGs. Overall, our study provides valuable insights into the optimal selection of BESS and the impact of ambient temperature on their performance, which can help in the development of more efficient and reliable MGs.

1. Introduction

Energy storage systems (ESSs) stock electricity when there is a surplus of electricity, or when electricity rates are low, and provide the stocked electricity to the unit when electricity is in high demand or prices are high. Therefore, for the successful functioning of power facilities, the algorithm development of an energy management system (EMS) is mandatory. Battery specifications and EMS design sizing have been thoroughly studied, as the battery represents a major part of the project cost when designing EMSs [1]. Such battery choice and control are important, as aging problems caused by improper battery management account for a large part of the total replacement budget. With the development of new sources of renewable energy [2–5], microgrids (MGs) and optimization techniques related to these areas have appeared. An MG [6–8] can be defined as an isolated or connected network that can produce electrical

energy from different hybrid sources and deliver or store it in an electrical ESS [9–11]. Several studies have already been carried out to develop the productivity of this type of network through the development of maximum power point tracking (MPPT) algorithms [12–14]. The development of these technologies requires a low ESS compatible with this type of network in terms of lifetime costs, response time, and the amount of energy produced [15–17]. There are several studies that have worked on the behavior and mode of operation of batteries, with electrical and physical modeling citing or demonstrating models of equivalent circuits of Li-ion batteries, while including mathematical equations characterizing their operational behavior. Similar research can be found with other types of batteries, such as lead-acid and nickel-cadmium [18–21]. Other studies have highlighted a comparative study between the different battery technologies applied in this field and technical-commercial studies [22]. These studies focused on investment costs, life span, and price of units and neglected the specific needs of MGs in terms of response time, recharge time, and operational safety. A comparison between the nature of batteries, their chemical compositions, and their manufacturing technology [23, 24] helps understand such a technology using chemical equations, materials layers, energy density, etc. However, each study focused only on one type of batteries. With the appearance of new concepts such as smart grids, MGs, battery ESSs (BESSs), and systems of network management [25, 26], it is required to operate the ESS in terms of density of energy compatibility with networks. In addition, some studies have compared the BEES applied in MGs, showing the operating behavior of certain types of batteries in MGs in terms of commercial technologies, chemical compositions, physical modeling, etc. However, there is a lack of results in terms of comparison between different charging technologies as regards climatic conditions, fast charging, and storage. The objective of this work is to investigate the impact of ambient temperature on the behavior of lithium-ion, lead-acid, and supercapacitor batteries in terms of state of charge (SOC) and response time as a function of power value. This work aims to fill this research gap by studying the behavior of different types of batteries under varying ambient temperature and power levels.

2. Presentation of the Used Approach

Several research studies have been conducted on energy storage systems on both technology and technical characteristics or on energy management systems and algorithms, such as MPPT or BMS for ESSs, without considering the different batteries used in MGs and their conditions and requirements.

This work presents the modeling of the different types of ESSs for MGs (Li-ion, lead-acid, nickel-cadmium, nickel-metal hybrid, and supercapacitor). This modeling starts by physical-electrical modeling for the different batteries studied. Then, a study of the recharging behavior with various levels of low/high current will make an analogy of fast recharge systems. This technology has become a scientific research field, where the recharging time became a key factor for system reliability. On the other hand, we validate the comparative study by applying a BMS system to observe the charging behavior and its effect on the SOC for each type. Moreover, the effects of the external conditions on the mode of operation of BESSs, such as the ambient conditions, the SOC, and the response time, have been studied.

Figure 1 shows a comparative study of the charging and discharging response time for fast-charging techniques and the effect of elevated temperature on battery operations, which is critical for understanding battery performance under different conditions. Charge and discharge rates can have a significant impact on battery performance. Rapid charging and discharging can increase the internal resistance of the battery, reduce its capacity, and shorten its life. Therefore, it is critical to evaluate the response time of rapid-charging techniques to determine their impact on battery performance. In addition, a high temperature can have a significant impact on battery performance. Heat can increase the internal resistance of the battery, reduce its capacity, and increase the rate of chemical reactions, which accelerates its aging. Therefore, it is essential to study the effect of elevated temperature on battery operations to determine the optimal operating temperature range. A comparative study of these factors can help to identify the most efficient and reliable battery technologies for various applications. For example, batteries used in electric vehicles require fast charge and discharge rates, but the effect of a high temperature on battery operations can be a limiting factor. Therefore, a comparative study can help to determine the optimal battery technology for that application.

3. BESS Modeling

There are many available battery designs developed by scientists with various intricacies to address battery performance for particular goals, e.g., battery design, performance estimation, and circuit simulation. Three main groups can be distinguished: electrochemical, mathematical, and electric models [27]. In order to better understand the operation mode of each type of ESSs, it is necessary to go through the physical/electrical modeling stage, which describes all the variables and characteristic parameters of different battery models. The variation in these parameters has an influence on the operation mode. This part of the work focuses on the physical modeling of the battery types already mentioned in the previous section.

3.1. Lead-Acid Battery Model. The modeling of lead-acid batteries as a complete system is based on the electrochemical ESS. However, due to the nonlinearities, interconnected reaction, and relationships involved, this approach requires significant computational power to simulate the entire system in detail [28]. Thevenin's model, shown in Figure 2, provides a simplified representation of the lead-acid battery behavior in an electrical circuit. This model represents the battery as a voltage source in series

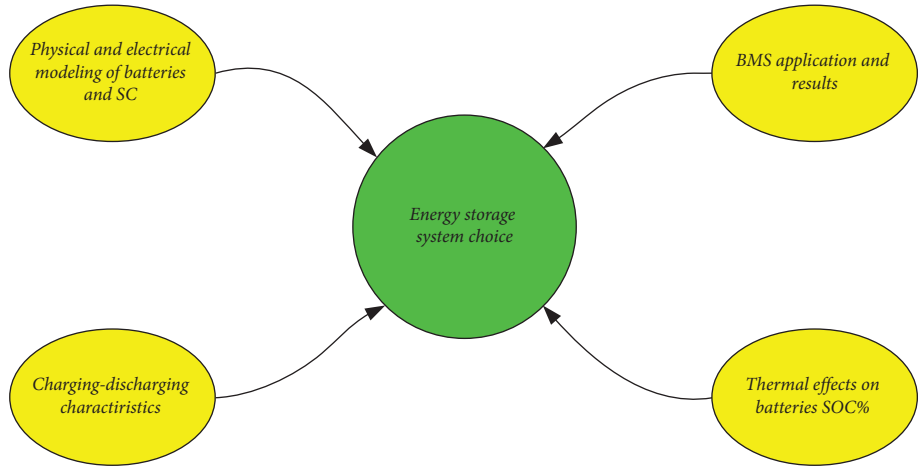

Figure 1: Strategy of optimal storage system selection.

with an internal resistance. The voltage source represents the battery's open-circuit voltage, which is the voltage measured when the battery is not being discharged. The internal resistance represents the resistance that the electric current encounters as it passes through the electrolyte and plates of the battery. The Thevenin model is useful for simulating and optimizing the battery performance under various conditions. By using this model, engineers and researchers can design BMS, predict battery life, and optimize battery performance. In summary, Thevenin's model is a simplified electrical model used to represent the behavior of a lead-acid battery in an electrical circuit, representing the battery as a voltage source in series with an internal resistance, which is useful for simulating and optimizing the battery's performance under different conditions.

Thevenin's model of a lead-acid battery can be represented by the following equation:

$$V = E - IR_i, \tag{1}$$

where V is the battery voltage, E is the open-circuit voltage of the battery, I is the current flowing through the battery, and R_i is the internal resistance of the battery.

The internal resistance of the battery can be expressed as

$$R_i = R_o + K_C \times \mathrm{SOC}, \tag{2}$$

where R_o is the resistance when the battery is fully charged, K_c is the capacity coefficient, and SOC is the state of charge of the battery.

The capacity coefficient can be expressed as

$$K_C = K_1 + K_2 \times \exp\left(-K_3 \times \mathrm{SOC}\right), \tag{3}$$

where K_1, K_2, and K_3 are empirical constants that depend on the battery chemistry and construction.

The SOC of the battery is a critical factor in determining the internal resistance and voltage of the battery. The calculation of the SOC should be as precise as possible. The SOC of the battery can be determined as the ratio of the amp-hours left in the battery to the total amp-hours of the battery, as shown in the following equation [30, 31]:

$$\mathrm{SOC} = 1 - \frac{\mathrm{AhD}}{\mathrm{Ah_{nom}}}. \tag{4}$$

The ampere hour discharged is given by equation (5), while the main reaction current in the battery (I_{mr}) and the ampere hour discharged at the start of the process are, respectively, given by equations (6) and (7):

$$\mathrm{Ah}_D = -\int I_{\mathrm{mr}}\mathrm{d}t + \mathrm{Ah_{Do}}, \tag{5}$$

$$I_{\mathrm{mr}} = I_{\mathrm{bat}} - I_{\mathrm{gas}}, \tag{6}$$

$$\mathrm{Ah_{Do}} = \mathrm{Ah_{nom}} - \mathrm{Ah_{nom}SOC_0}. \tag{7}$$

The typical gravity of the battery is very important for the internal or open-circuit voltage. It is calculated through

$$\mathrm{SG} = \mathrm{SG_{full}} - \frac{\mathrm{Ah}_D\left(\mathrm{SG_{full}} - \mathrm{SG_{empty}}\right)}{\mathrm{DK}}, \tag{8}$$

$$V_{\mathrm{oc}} = 0.84 + \mathrm{SG}.$$

The gassing effect causes a loss of energy in the battery. The gassing current under a load status is given by

$$I_{\mathrm{gas}} = I_{g0} - \exp\left(C_u \times \left(V_{\mathrm{bat}} - 2.23\right)\right). \tag{9}$$

The internal resistance during charging and discharging operations is a result of the SOC, the type of the electrolyte, and the electrodes. It is given by

$$R_i = \frac{V_{\mathrm{bat}} - V_{\mathrm{oc}} - V_{\mathrm{dl}} - V_d}{I_{\mathrm{mr}}}, \tag{10}$$

where

$$V_{\mathrm{bat}} = V_{\mathrm{oc}} + I_{\mathrm{mr}}R_i + V_{\mathrm{dl}} + V_d. \tag{11}$$

The Thevenin model of lead-acid has, however, some disadvantages, such as not considering the battery's nonlinear behavior and the dependency of its internal resistance on SOC and temperature. In contrast, the RC model of the lead-acid battery considers the battery's nonlinear behavior

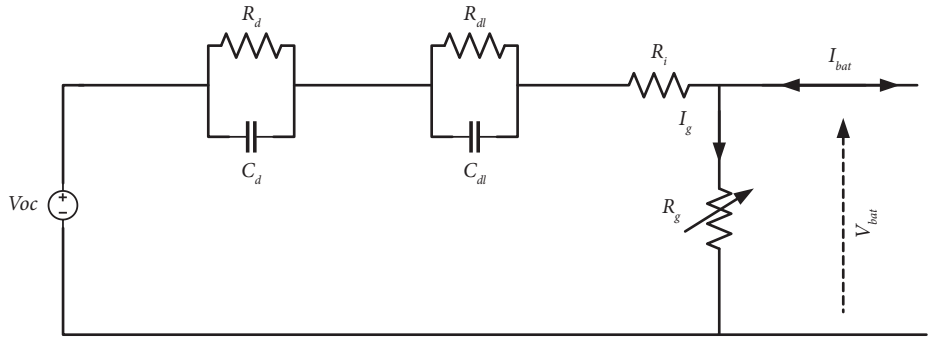

Figure 2: Electric model of the lead-acid battery [29].

and the effect of the temperature and SOC on its internal resistance. This model includes a resistor and a capacitor in series with a voltage source, representing the battery's internal resistance and capacitance, respectively. The voltage across the capacitor represents the battery's terminal voltage, and the current flowing through the resistor represents the internal current of the battery. Compared to Thevenin's model, the RC model is considered more trusted due to its ability to accurately capture the battery behavior and dynamics under various operating conditions. This model is widely used in BMS and simulation software, as it provides a more accurate representation of the battery behavior and as it can predict its performance more accurately. Therefore, when considering the simulation and modeling of lead-acid batteries, the RC model is often preferred over Thevenin's model.

The RC model of a lead-acid battery is a widely used electrical model to represent battery behavior in an electrical circuit. It comprises a voltage source, internal resistance, and a capacitor in series, which represent the open-circuit voltage, the resistance to current flow and the charge storage capacity of the battery, respectively. The equations governing the model describe the voltage across the battery terminals as a function of the open-circuit voltage, current, resistance and charge stored in the battery. The open-circuit voltage is dependent on the SOC and temperature of the battery. Figure 3 shows the equivalent circuit of the RC model, which includes two RC branches.

The model is composed of a voltage source in series with an internal resistance and a capacitor. In a more advanced version of the model, there are two RC branches [32–34]. The voltage source represents the battery's open-circuit voltage, while the internal resistance represents the resistance that the electric current encounters as it passes through the electrolyte and plates of the battery. The two RC branches represent the charge transfer resistance and diffusion resistance within the battery, respectively.

The mathematical equations for the two-branch RC model of a lead-acid battery are as follows.

The voltage across the battery terminals at time t is given by

$$V(t) = V_{oc}(t) - I(t) \times \frac{(R_0 + R_1)}{C_1}. \tag{12}$$

The charge stored in the first RC branch at time t is given by

$$Q(t) = C_2 \times V_2(t). \tag{13}$$

The voltage across the second RC branch at time t is given by the following equation:

$$V_2(t) = I(t) \times R_1 + V_1(t), \tag{14}$$

V_1 is the voltage across the first RC branch given at time t by

$$V_1(t) = I(t) \times R_0 + V_c(t), \tag{15}$$

where:

$$V_c(t) = \frac{1}{C_0} \times \int_0^t I(t')\mathrm{d}t'. \tag{16}$$

The charge Q stored in the first RC branch is related to voltage V_1 by the following equation:

$$Q(t) = C_1 \times V_1(t). \tag{17}$$

3.2. Li-Ion Battery. Due to the increasing use and continuous technological improvement in Li-ion batteries, the battery design is a valuable tool for various research and product development tasks. Studies such as battery designs can be categorized into electrochemical and equivalent circuit designs [35]. The mathematical relation of the cells of a lithium-ion battery to their V-I property, the SOC, the internal resistance, the duty cycle, and the self-discharge is represented in a lithium-ion battery model. The equivalent circuit design of a lithium-ion battery is a design performance model that uses one or more parallel combinations of resistance, capacitance, and other circuit components to build an electrical circuit in order to reproduce the dynamic characteristics of Li-ion batteries. Equation (18) states that the terminal voltage v is instantaneously proportional to the open-circuit voltage V_{oc} [35, 36]:

$$v(t) = V_{oc}. \tag{18}$$

The SOC of a cell is 100% when the cell is completely charged, and the SOC is 0% when the cell is completely discharged. The quantity of charge dropping from 100% to 0% is the full capacity measured in Ah or mAh. Figure 4

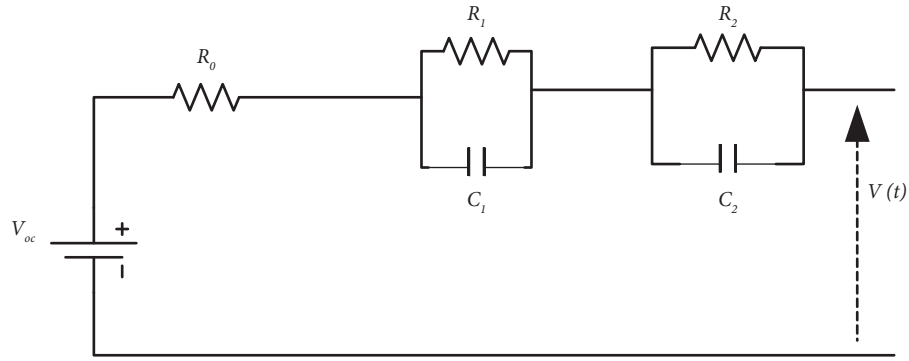

Figure 3: Precise electrical model for lead-acid battery.

illustrates the common battery design used. It is an ideal battery with an open-circuit voltage V_{oc}, a constant equivalent internal resistance R_{int}, and a terminal voltage $v(t)$. Once fully charged, the terminal voltage $v(t)$ can be measured by measuring the open-circuit voltage, and R_{int} can be measured by attaching a load and sensing both the terminal voltage and the current.

A fully charged battery has a much greater open-circuit voltage than a discharged battery. The design of R_{int} seems quite straightforward, but it overlooks the variable character of the internal resistance related to the temperature, the SOC, and the electrolyte concentration. Figure 3 depicts the circuit schematic of Thevenin's resistive battery design. This design has two kinds of internal resistances, R_0 and R_1, which are, respectively, related to the charge and discharge characteristics of the battery. The electrical and nonelectrical leakage losses are modeled by the internal resistance R_0 and R_1. The scattering voltages can also be precisely derived using one or more parallel RC branches. This method gives better results than the R_{int} method, but transient states such as the effect of capacitance are not taken into consideration. Therefore, this model is nondynamic and not suitable for applications involving electrical vehicles and hybrid electrical vehicles. In a relaxation mode, the voltage progressively decreases to zero, which is called the diffusion voltage that can be accurately approximated using parallel RC branches:

$$v(t) = V_{oc}(z(t)) - i(t)R_{int} - V_{C1}(t). \tag{19}$$

Figure 5 presents a precise design of an electric battery, modeling of the battery capacity, the SOC, and the operating time using a capacitor and a current-controlled source. The circuit considers battery life as well as its slow and fast transient responses. A voltage-controlled source as a function of SOC is used to break the barrier between SOC and V_{oc}.

3.3. Supercapacitor. Supercapacitors, situated in the mid-hierarchy of energy storage units, have some key advantages that make them essential for applications that need high-power delivery in a small amount of time. Determining the suitability of strategies for the use of these devices involves understanding the characteristics of the supercapacitor

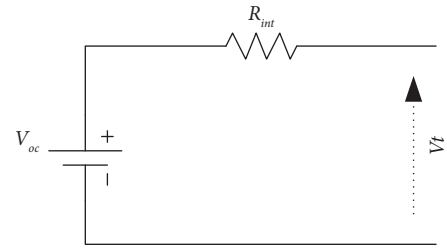

Figure 4: Thevenin's equivalent circuit battery model.

under different loads and its control [37]. The double-layer capacitor is a physical device that has not only a required capacitance but also an inevitable parasitic inductance thanks to its physical geometry. It also has a series resistance caused by the ohmic resistance of the electronic and ionic conductors, as well as a parallel resistance caused by the leakage current between the electrodes. On the other hand, it can be modeled by an RC branch, where the capacitor is represented by the capacitance C, the series resistance by R_S, and the parallel resistance by R_P. The RC circuit equation [38–40] is given by

$$V = \frac{Q}{C} + R_S \times \frac{dQ}{dt} + R_P \times I_{Leak}, \tag{20}$$

where V is the voltage across the supercapacitor, Q is the charge stored in the capacitor, and I_{Leak} is the leakage current. The voltage response of the RC model for a supercapacitor can be described by the following equation:

$$V(t) = V_0 \times \exp\left(\frac{-t}{R_{eq} \times C_{eq}}\right), \tag{21}$$

where $V(t)$ is the voltage across the supercapacitor at time t, V_0 is the initial voltage, R_{eq} is the equivalent resistance of the supercapacitor (Rs + Rp), and C_{eq} is the equivalent capacitance of the supercapacitor. Equation (21) shows that the voltage across the supercapacitor exponentially decays with time, with a time constant given by the product of R_{eq} and C_{eq}. The value of R_{eq} and C_{eq} can be determined experimentally or through modeling and simulation.

However, in real cases, we cannot represent a supercapacitor solely from an RC assembly. In certain situations, it is not sufficient to simulate a real supercapacitor only by

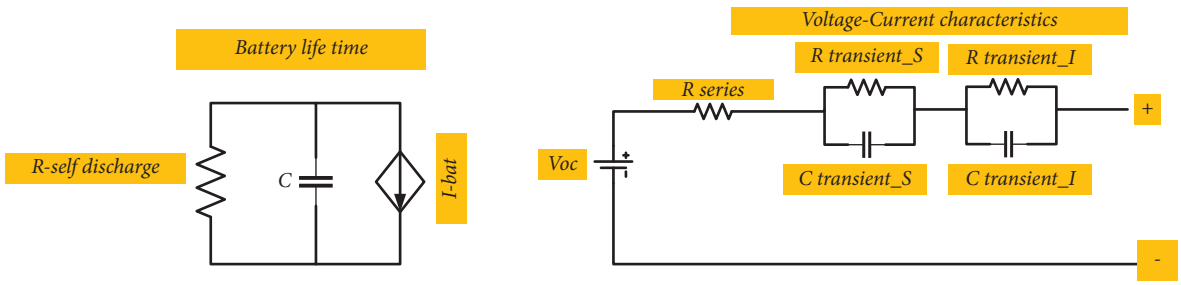

Figure 5: Precise electrical model of Li-ion battery.

one of the RC models discussed above. The designs listed previously can be extended to a more generic model. The number of branches can be optimally extended to infinity. In addition, the supercapacitor has an inductance effect that must also be modeled, particularly at higher operating frequencies. Finally, the leaking current effect has been ignored in previous designs. Figure 6 shows a typical RC circuit design with parallel shunting. In this figure, resistor R_p stands for the leakage current losses, and the series inductance L gives the high-frequency inductance effect.

The equivalent impedance (Z_{eq}) of the RC model of a supercapacitor can be calculated using the following equation:

$$Z_{eq} = R + \frac{1}{(jC\omega)}, \tag{22}$$

where R is the series resistance, C is the capacitance of the supercapacitor, ω is the angular frequency of the AC signal, and j is the imaginary unit. The first term R represents the ohmic resistance of the supercapacitor, whereas the second term $1/(jC\omega)$ represents the capacitive reactance. The impedance of the supercapacitor is frequency-dependent, decreasing as the frequency increases due to the decrease in the capacitive reactance.

To obtain high power, it is absolutely necessary to have a low ESR. The parallel resistance Rp only has a visible effect at very low frequencies (below the millihertz range). It is responsible for the self-discharge time of the capacitor. Its value must be as high as possible to limit the leakage current. The self-discharge time constant t is equal to $\tau = C \times \mathrm{Rp}$.

3.4. Nickel-Metal Hybrid and Ni-Cd Battery Models. Ni-Mh and Ni-Cd are the type of reloadable batteries, whose chemical reaction is the same [41]. The only difference between these two batteries is that the capacity of Ni-Mh is 2 or 3 times as big as that of Ni-Cd. The electrical modeling of Ni-Mh is like that of Ni-Cd, derived by Notten and based on [42]. Figure 7 demonstrates the model of the battery, where E_{Nieq} and E_{Meq}, respectively, represent the balance voltages of the nickel and metal electrodes, R_{Ni} and R_M are, respectively, the connection resistances of the nickel and metal electrodes, R_e is the resistance of the electrolyte, and $C_{\mathrm{dt\text{-}Ni}}$ and $C_{\mathrm{dt\text{-}M}}$ are the double-layer capacitors. The diodes represent the charge-transfer phenomenon. The combination of ($C_{\mathrm{diff\text{-}Ni}}//R_{\mathrm{diff\text{-}Ni}}$) and ($C_{\mathrm{diff\text{-}M}}//R_{\mathrm{diff\text{-}M}}$) is related to the diffusion effect.

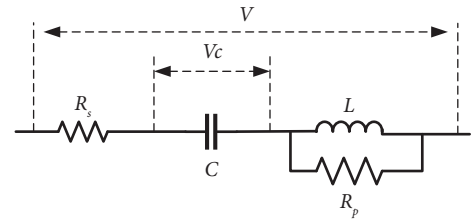

Figure 6: Electrical equivalent circuit of the basic supercapacitor.

4. Results and Discussion

This part of the work highlights the effect of changing the supply current of BESSs and their effect on the charging/discharging behavior, where it focuses on the change of the SOC of each type of energy storage system. This indicates by analogy of the system response time, where the latter sets a key factor in the design of the MG. This is because some users require a very fast response time for the charging and discharging phases. Furthermore, this kind of simulation offers the opportunity to observe two vital parameters for all ESS types, which are depth of charge (DOC) and depth of discharge (DOD). These two factors have a relation to the life span of the batteries and their operational status. The cycling conditions, such as the number of frequent discharging/charging events and the charging/discharging rates, have a great impact on the battery lifetime [43]. In the second part, the results of the use of BMS are presented and discussed. The BMS is essential to ensure the safe and reliable operation of the batteries [44] and for the implementation of the ESS in the system. An in-depth review of the years 2006 to 2020 is performed in the area of BMSs. Several functions, advantages, and disadvantages of the approaches used in the BMS for cell equilibration, thermal control, battery overvoltage and overcurrent protection, state-of-health estimation, and battery SOC estimation are discussed. In addition, some critical deficiencies are identified, and a framework for the design of an effective BMS is suggested. The implementation of smart technologies, such as a digital twin of a battery, cyber-physical systems, battery swap technologies, nondestructive testing, self-reconfigurable batteries, and prudent recycling/reuse through automation are also addressed. In summary, critical gaps, advanced technologies, and the framework that researchers can use to build complete systems including advanced BMSs, real-time battery monitoring, and battery reuse and recycling as a complete

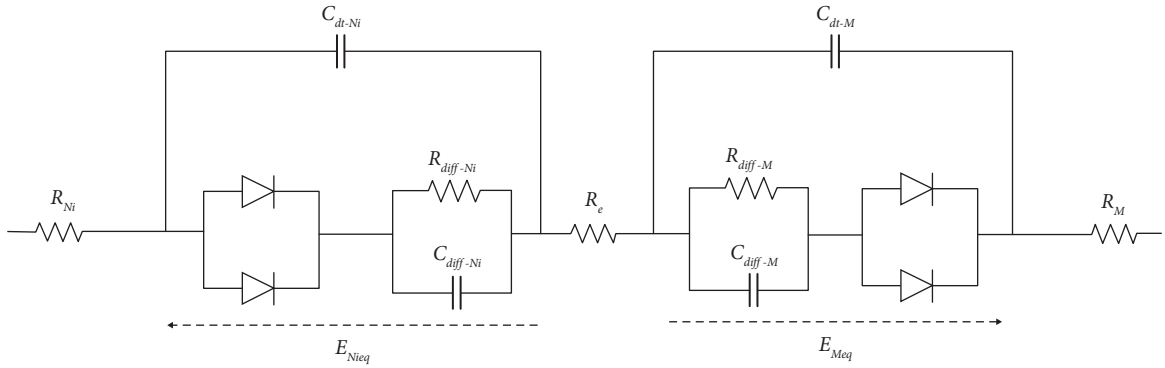

Figure 7: Battery model of Ni-MH based on the Notten model for Ni-Cd.

unit are presented [45]. In the last part of simulation, the work is directed towards the effect of an external factor which has a great influence on the mode and working behavior of the BESS, which is the ambient temperature. This factor has an impact on battery aging.

4.1. BESS Charging/Discharging Behavior. In this section, we compare the response time of the studied BEESs with identical dimensions. These systems have a capacity of 48 Ah and 12 V for batteries and 500 Farad and 48 V for the supercapacitor and are subjected to a variable continuous current. The charge/discharge response time of each type of BEES is simulated using MATLAB/Simulink software.

From Figures 8 and 9, it is shown that Li-ion batteries and SCs have the fastest charging time compared to other BEESs. For instance, at $t = 90$ s, the SOC of Li-ion batteries is approximately 12%, and they have a steeper recharge slope than the other BEESs. The closest candidate is lead-acid batteries, with an SOC of approximately 10% under the same conditions and period. However, Ni-Mh and Ni-Cd have an SOC of less than 10% at this instant. Therefore, for fast charging, Li-ion batteries are the preferred choice. However, if we consider the speed of recharging with energy density, Li-ion victory is uncertain. Under the same simulation conditions, at $t = 90$ s, the supercapacitor with a capacity of 500F reaches almost 80% of the SOC (see Figure 9), with a significant slope. Therefore, to design an energy storage system with a rapid response to recharging and high-energy density, we must use a combination of Li-ion batteries and SCs.

Figures 10 and 11 present the response time of the different BESSs and the supercapacitor under variable loads. At $t = 70$ s, the discharge phase ends as the SOC of Li-ion reaches approximately ±94%, the SOC of lead-acid reaches approximately ±95%, and the SOC of Ni-Cd reaches 95%. Indeed, both the SOC of Ni-Mh and the SOC of the supercapacitor are below 60%. Based on these results, the combination of Li-ion batteries and SCs is validated as the optimal choice, as previously discussed.

The charging and discharging of an ESS can be represented by a charge/discharge curve, as shown in Figure 12. Fast charging techniques may lead to variations in the charge/discharge curve of different types of batteries, such as Li-ion, lead-acid, Ni-Cd, Ni-Mh, and supercapacitors, due to differences in their chemistry, construction, and operating conditions. The depth of charge and discharge and the response time are crucial factors that impact battery performance. The depth of charge refers to the amount of energy that can be stored in the battery, while the depth of discharge refers to the amount of energy that can be released. The response time is the duration required for the battery to reach its complete SOC or state of discharge, influenced by factors such as the charging/discharging rate, temperature, and battery health. The ESS charging/discharging curve is an essential tool for assessing the performance of different batteries and supercapacitors. When utilizing fast-charging techniques, it is vital to consider the depth of charge and discharge, the response time, and the potential impacts on the battery performance and life span.

4.2. Mathematical Modeling and Simulation of Battery Faults in Energy Storage Systems. The use of failure models in battery simulation research offers many advantages. By incorporating realistic failure conditions, these models enable more accurate and representative simulations of battery behavior. Researchers can assess battery performance under various failure scenarios, such as capacity decay or increased internal resistance, providing valuable information on the impact of failures. Failure simulations help diagnose specific failure patterns and can be used to optimize battery design for improved fault tolerance and safety. Running simulations with failure models is cost-effective and accelerates research progress by effectively exploring multiple failure scenarios. In addition, robust failure models prepare researchers to meet future challenges in battery technologies, contributing to the development of reliable and efficient energy storage solutions for a variety of applications.

In this section, we present mathematical models for different battery types, including Li-ion, lead-acid, supercapacitor, Ni-Cd, and Ni-Mh batteries. These models account for the behavior of faulty batteries under various conditions, such as capacity decay and increased internal resistance. The mathematical equations describe the response of battery voltage over time, taking into account the specific characteristics and parameters of each battery type. By integrating these failure models into a simulation

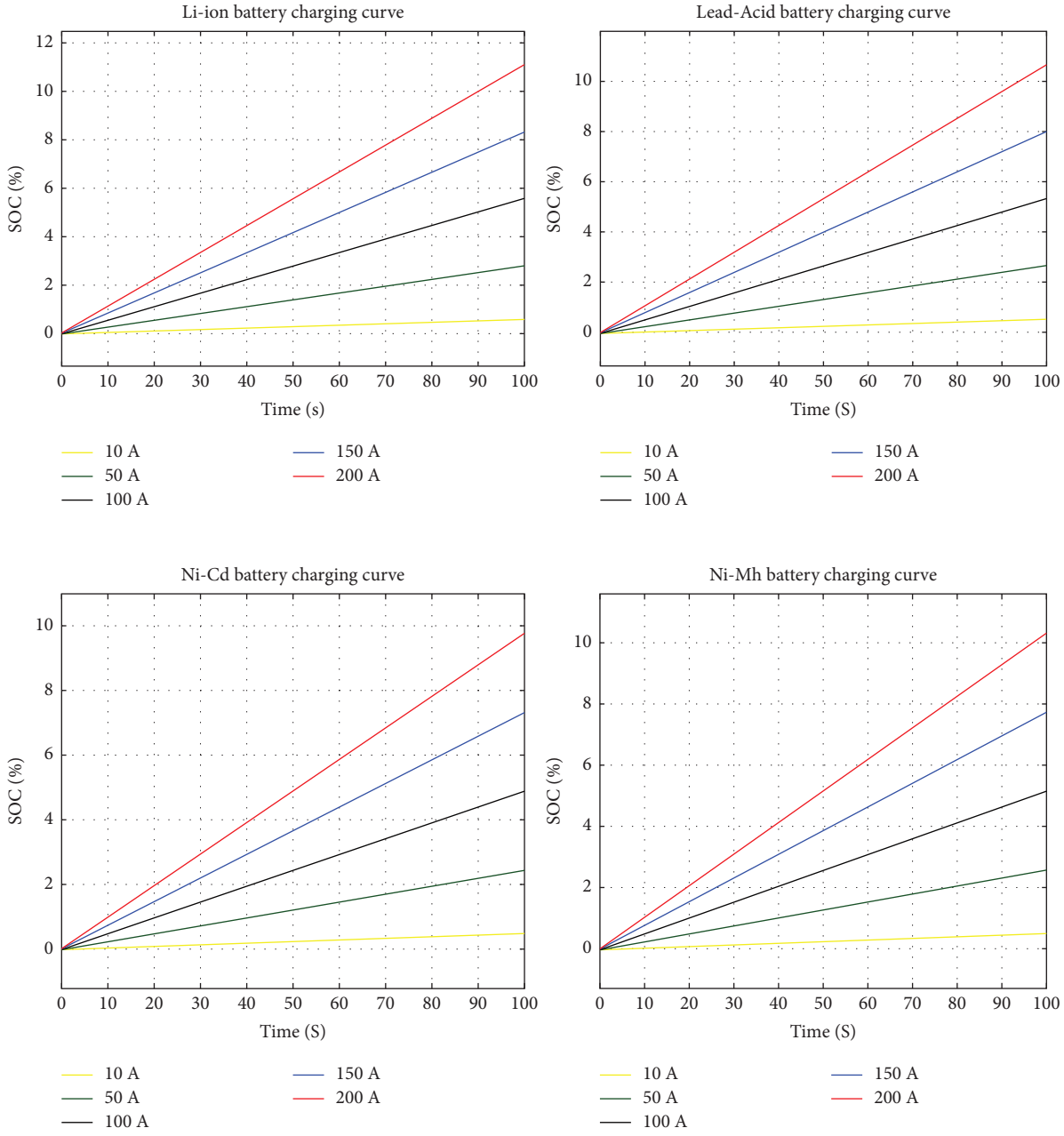

Figure 8: Battery charging behavior.

framework, we can simulate and analyze the performance of faulty batteries in energy storage systems. The simulation framework provides a powerful tool for assessing the impact of battery failures on system performance, such as voltage degradation, power output reduction, and energy efficiency. It enables us to evaluate the effectiveness of different fault mitigation strategies and optimize the operation of energy storage systems in the presence of faulty batteries. By performing simulations under various operating conditions and failure scenarios, we can better understand the behavior of faulty batteries and make informed decisions regarding battery management and system design.

Overall, this section presents a comprehensive approach to the mathematical modeling and simulation of battery faults in energy storage systems. It highlights the importance of accurately representing battery faults in simulations in order to assess their impact on system performance and guide the development of robust and reliable energy storage systems. The results of these simulations can inform the design and optimization of battery management strategies,

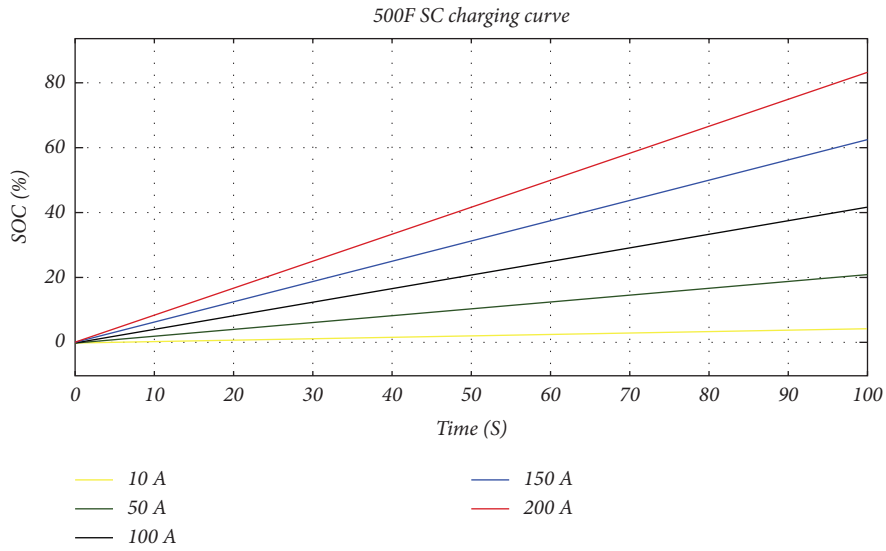

Figure 9: 500F supercapacitor charging curve.

helping to improve the performance and longevity of energy storage systems in a variety of applications.

(1) Capacity fade (Li-ion battery) [46, 47]:

(i) The effective capacity C_{eff} of the battery can be modeled as a decreasing function over time or cycles, such as

$$C_{\text{eff}}(t) = C_{\max} \times (-k \times t), \tag{23}$$

where C_max is the initial maximum capacity and k is a degradation rate constant.

(2) Internal resistance increase (Li-ion battery) [48, 49]:

(i) The internal resistance ($R_{\text{int}}(t)$) of the battery can be modeled as an increasing function over time or cycles, such as

$$\mathbf{R_{int}}(\mathbf{t}) = \mathbf{R_{initial}} \times (\mathbf{1} + \mathbf{k} \times \mathbf{t}), \tag{24}$$

where R_{initial} is the initial internal resistance and k is a degradation rate constant.

(3) Sulfation (lead-acid battery) [50–52]:

(i) The effective capacity (C_{eff}) of the battery can be modeled as a decreasing function due to sulfation, such as

$$\mathbf{C_{eff}}(\mathbf{t}) = \mathbf{C_{max}} \times (-\mathbf{k} \times \mathbf{t}), \tag{25}$$

where C_max is the initial maximum capacity and k is a degradation rate constant.

(4) Electrolyte stratification (lead-acid battery) [53, 54]:

(i) The effective conductivity and diffusion properties of the battery can be modeled as spatially varying functions to represent electrolyte stratification effects.

(5) Capacitance loss (supercapacitor) [55, 56]:

(i) The effective capacitance (C_{eff}) of the supercapacitor can be modeled as a decreasing function over time or cycles, such as

$$C_{\text{eff}}(t) = C_{\text{initial}} \times (-k \times t), \tag{26}$$

where C_initial is the initial capacitance and k is a degradation rate constant.

(6) Increased equivalent series resistance (ESR) (supercapacitor) [57, 58]:

(i) The equivalent series resistance (ESR) of the supercapacitor can be modeled as an increasing function over time or cycles, such as

$$\text{ESR}(t) = \text{ESR}_{\text{initial}} \times (-k \times t), \tag{27}$$

where ESR_initial is the initial ESR and k is a degradation rate constant.

(7) Fault model for the Ni-Cd battery [59, 60]: the capacity fade fault for a Ni-Cd battery can be represented mathematically as follows:

Capacity fade fault model: Let C_max be the maximum capacity of the Ni-Cd battery (in Ah). Let C_fade be the reduced capacity due to capacity fade (e.g., C_fade = 0.8 for 80% capacity retention). Let V_nominal be the nominal voltage of the Ni-Cd battery (e.g., V_nominal = 1.2 V per cell). Let t be the time in seconds.

The voltage across the Ni-Cd battery with capacity fade can be expressed as

$$V\_\text{capacity\_fade\_nicd} = \frac{(C\_\text{fade} \times C\_\text{max})}{C\_\text{max} \times V\_\text{nominal}}. \tag{28}$$

(8) Fault model for the Ni-Mh battery [61–63]: the increased internal resistance fault for a Ni-Mh battery can be represented mathematically as follows:

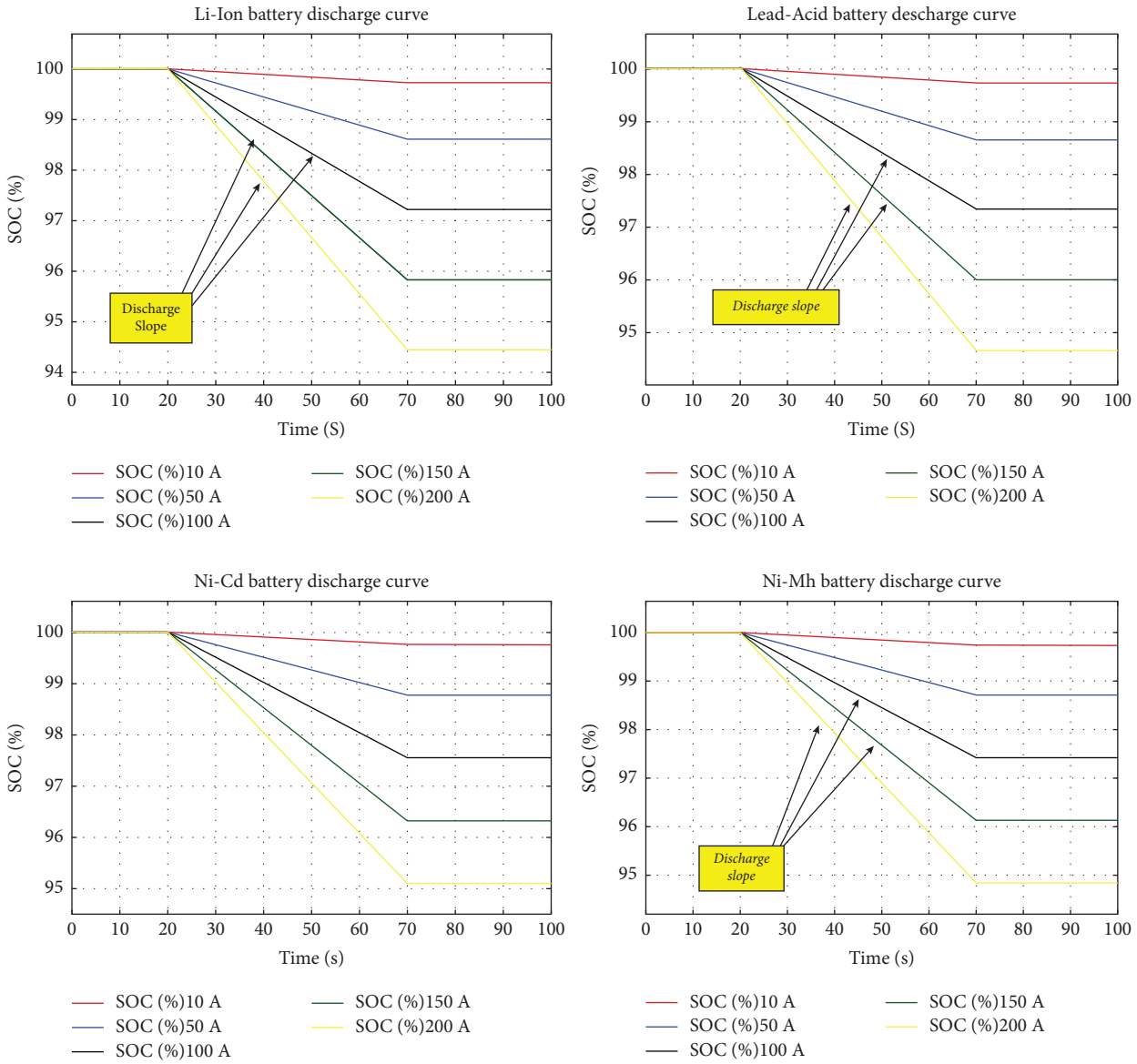

Figure 10: Discharging behavior of batteries.

Increased internal resistance fault model: Let V_nominal be the nominal voltage of the Ni-Mh battery (e.g., V_nominal = 1.2 V per cell). Let R_int_nominal be the nominal internal resistance of the Ni-Mh battery (e.g., R_int_nominal = 0.01 ohms). Let R_int_fault be the increased internal resistance due to the fault (e.g., R_int_fault = 0.02 ohms). Let t be the time in seconds.

The voltage across the Ni-Mh battery with increased internal resistance can be expressed as

$$V\_\text{internal\_resistance\_nimh} = V\_\text{nominal} - R\_\text{int\_fault} \times 0.1 \times t. \tag{29}$$

The developed MATLAB code provides a comprehensive battery modeling framework for simulating the behavior of different battery types, including Li-ion, lead-acid, supercapacitor, Ni-Cd, and Ni-Mh. It allows for the characterization of normal battery operation as well as the introduction of fault models, such as capacity fade and increased internal resistance. By specifying the battery model parameters and utilizing voltage equations, the code enables the analysis of battery voltage variations over time. The resulting plots showcase the comparison between normal and faulty battery scenarios, offering valuable insights into the impact of these faults on battery performance. This code

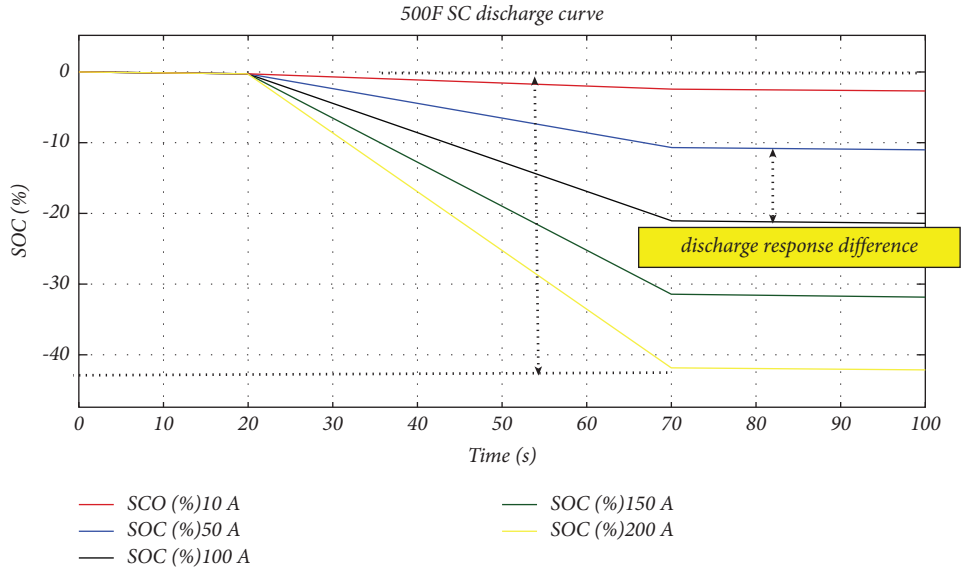

Figure 11: Supercapacitor discharge curve.

serves as a valuable tool for understanding and evaluating the behavior of various batteries, facilitating research and development efforts in the field of energy storage systems. Figures 13–17 describe the behavior of fault batteries compared to normal one in the same working conditions.

Simulation results demonstrated the effectiveness of the proposed battery fault models for different battery types, including Li-ion, lead-acid, supercapacitor, Ni-Cd, and Ni-Mh. The voltage-time curves of each battery type in normal operation and under fault conditions were analyzed, highlighting the impact of capacity decay and increased internal resistance on battery performance. The simulation results validated the importance of taking faulty battery behavior into account in the design of energy storage systems, particularly in microgrid applications.

By incorporating failure models into our simulation framework, we gain valuable insights into the behavior of energy storage systems under various failure scenarios. These failure models enable us to study the robustness and reliability of proposed fast-charge strategies and to assess system response under failure conditions. In addition, the simulation results highlight the importance of selecting the right battery types and strategies to optimize microgrid performance and ensure their smooth operation in real-life environments.

4.3. Battery Simulator Test. The process of simulating battery behavior stands as a cornerstone in modern energy research and development. Within our comprehensive battery simulator test platform, we offer a seamless solution for replicating the performance of a wide array of battery cells housed in our extensive database. By a simple selection from the dropdown menu, researchers gain access to an array of prestored cells, each ripe for simulation, as exemplified in Figure 18. In a practical demonstration, we harnessed the power of controlled pulses, generating 50 ampere-hours (Ah) for charging and an equal and opposite −50 Ah for discharging, thus emulating the dynamic charging and discharging phases of an NCA lithium cell. This section ventures into the heart of battery simulator testing, exploring how it empowers researchers to scrutinize and fine-tune battery performance under diverse conditions. The ensuing figures (Figure 19 for discharging and Figure 20 for charging) present the simulation outcomes, vividly capturing the essence of these critical battery phases for existing cells.

4.4. Application of BMS on Behavior of ESS. The integration of an optimization of ESSs more specifically improves the battery-charging mode. An algorithm controls a converter which applies a rapid-charging mode [62] of the batteries and SC. Either it will play on the recharging frequency parameter or the converter is controlled by a PWM generator which will modulate the signal coming from the DC source. This technique can be also used in EV stations [63]. For the configuration of the systems, the initial SOC of the different BESSs must be at 10%. The systems go through four phases (stand-by, recharge, discharge, and stand-by) for the period ([0, 10 s], [10 s, 50 s], [50 s, 90 s], and [90 s, 100 s]), which gives an overview of the operating mode of the BESS managed by the BMS.

Figure 21 presents the algorithm for battery charge and discharge management. The BMS oversees monitoring and controlling various battery parameters, such as the SOC, current, voltage, and temperature, to optimize its performance and extend its life. The BMS can improve battery performance by ensuring that the battery is charged and discharged within safe limits and avoiding overcharging and overdischarging. This allows the battery to achieve higher SOC levels than without the BMS, as the BMS can accurately measure the battery SOC and control the charge/discharge process to optimize its performance. In addition, the BMS can also help balance the cells in the battery, ensuring that each cell is charged and discharged equally. This prevents cell imbalance and extends the life of the battery. Overall, the charge/discharge curve of a BESS managed by a BMS can

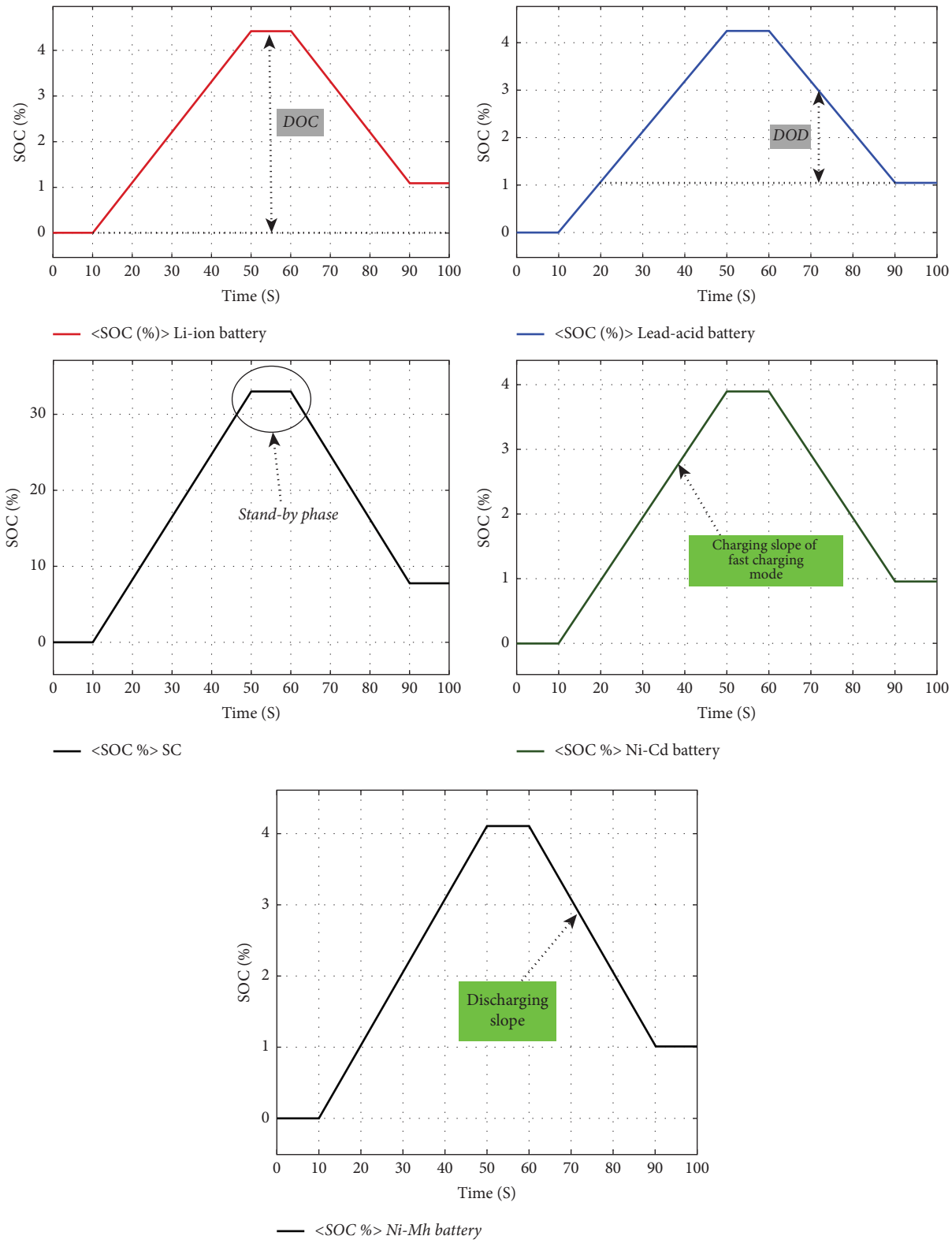

Figure 12: ESS charging/discharging curve.

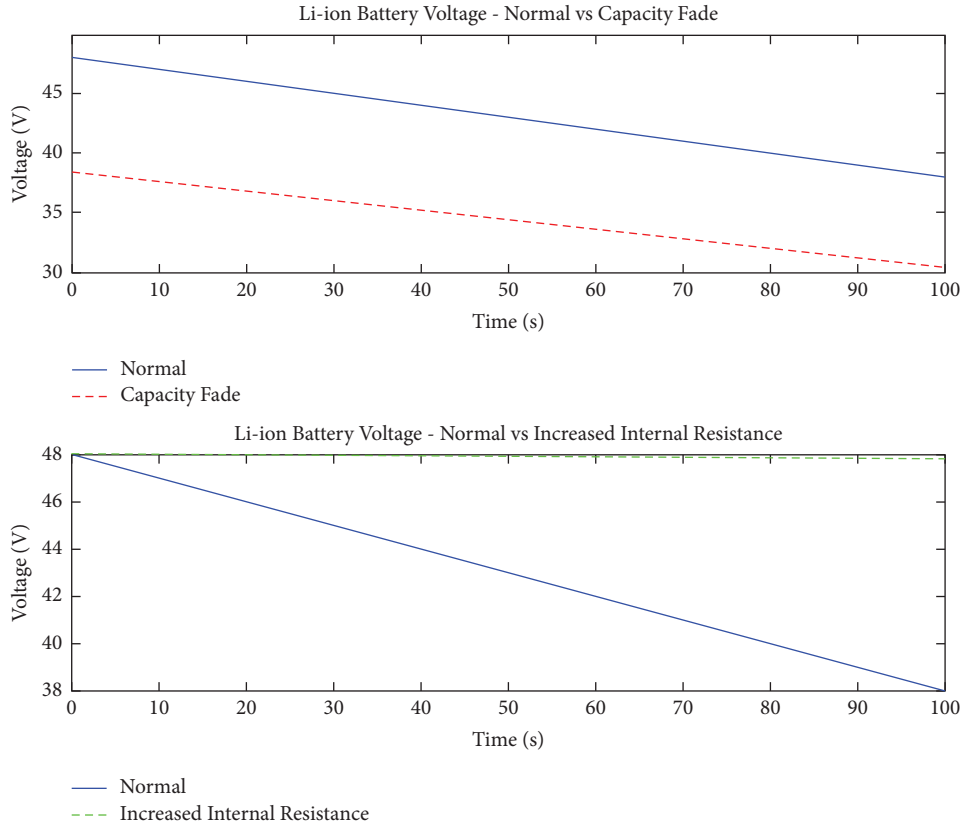

Figure 13: Li-ion battery voltage: normal vs. capacity fade.

demonstrate the benefits of using a BMS to monitor and optimize battery performance. The BMS can help the battery achieve higher SOC levels, extend the life of the battery, and ensure that it is operating securely and effectively.

In Figure 22, the response of the different BESSs to recharge/discharge is shown, but in a mode controlled by the BMS. For the response to the load, the proposed algorithm improves the response of Ni-Mh and Ni-Cd and on everything for the lead-acid battery that can be seen over the period between [10 s-90 s]. On the other hand, for the response to the discharge, the Li-ion battery is the best solution, which is demonstrated in the last phase (stand-by) for the period [90, 100 s] and the discharge phase between [60, 90 s].

4.5. Effect of Ambient Temperature on Charging and Discharging Behavior of Batteries. Simulation takes another path, where the work focuses on the effect of ambient temperature on the mode and behavior of the BESS work, more precisely on the SOC and the internal cell temperature [64]. Figure 23 shows that the BMS algorithm considers ambient temperature as a critical parameter and adjusts the charge and discharge parameters accordingly. The algorithm continuously monitors the battery temperature and adjusts the charge and discharge current limits to keep the temperature within a safe range. When temperature is too high, the algorithm reduces the charge current to prevent overcharging and the discharge current to prevent overdischarging, as these conditions can cause thermal runaway and damage the battery. On the other hand, when temperature is too low, the algorithm increases the charge and discharge current to maintain battery performance and avoid self-discharge.

Figure 24 presents the simulation results of the influence of the ambient temperature on the SOC of batteries. When varying the ambient temperature of the function of the lead-acid battery, it observes a slight increase in the DOC between time $t = 3000$ s and $t = 4000$ s. It also observes a rise in the sensitivity of response to recharge at $T = 80^{\circ}$C (the recharge slope) compared to $T = 25^{\circ}$C. On the other hand, with the increase in temperature, it observes a decrease in the DOD and consequently a decrease in temperature less than 0°C (in the present case, the simulation is performed at $T = -25^{\circ}$C and $T = 80^{\circ}$C), which improves the sensitivity of battery discharge, hence the low response time for the request of the load.

Another test highlights the effect of temperature on the mode of operation of the Li-ion battery when compared with another battery of the same type with a mode of operation at stable temperature at $T = 25^{\circ}$C. These tests are described below for different cases.

4.5.1. Case 1 ($T = \pm 60^{\circ}$C). The experiment demonstrates the temperature-dependent performance of the Li-ion battery model (battery A) when the surrounding temperature goes from 60°C to −60°C and then to 0°C. Battery B is the case where the impact of temperature is ignored. The results of the experiment are visualized in Figure 25, which compares the variation in the SOC between the two batteries at varying ambient temperature, and in

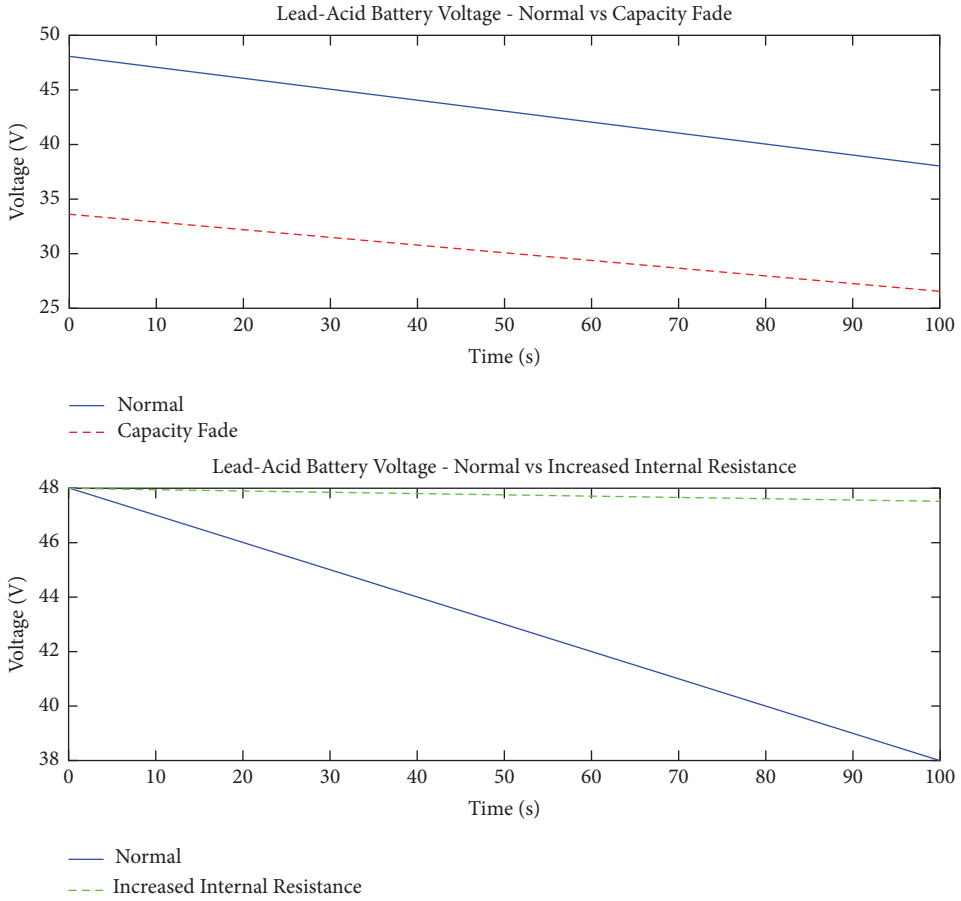

Figure 14: Lead-acid battery voltage: normal vs. capacity fade.

Figure 26, which shows the effect of the ambient temperature on the internal temperature of the battery cells. The results are shown as follows:

(i) At $t = 0$ s, batteries A and B discharge with 2 Amp at an air temperature of 60 C.

(ii) At $t = 150$ s, the core temperature climbs to its steady-state value of 29.2°C due to heat dissipation from the discharge operation. This results in a slight increase in the output voltage of battery A, while the output voltage of battery B continues to decline.

(iii) At $t = 1000$ s, the environmental temperature is dropped to −60°C. This leads to a sharp fall in the output voltage of battery A as the core temperature declines fast. In addition, the SOC of the battery decreases due to the capacity reduction. The output voltage of battery B keeps on going down gradually until it reaches its equilibrium voltage.

(iv) At $t = 2000$ s, the room temperature goes from −60°C to 0°C. As the internal temperature rises, the output voltage of battery A goes up. Moreover, as the capacity increases, the SOC of the battery grows. The output voltage of battery B remains constant up to its steady-state value.

(v) At $t = 2500$ s, batteries A and B are charged with 3 Amp at an environmental temperature of 0°C. This leads to an elevation of the internal temperature due to heat dissipation during the charging procedure, which raises the charging voltage of battery A. Then, batteries A and B continue to charge until they are completely charged.

The above experiment exhibits the impact of ambient temperature on the performance of both battery A and battery B. The temperature-dependent battery A exhibits variations in the output voltage and the SOC as a function of the ambient temperature, while battery B demonstrates a consistent discharge behavior.

4.5.2. Case 2 ($T = \pm 80$°C). The experiment illustrates the response of the model temperature-dependent lithium-ion battery (battery A) when the surrounding temperature ranges between 80°C and −80°C and then at 0°C. Battery B is the case where the effect temperature is neglected. The results of the experiment are visualized in Figure 27, which compares the variation in the SOC between the two batteries at varying ambient temperature, and in Figure 28, which shows the effect of the ambient temperature on the internal

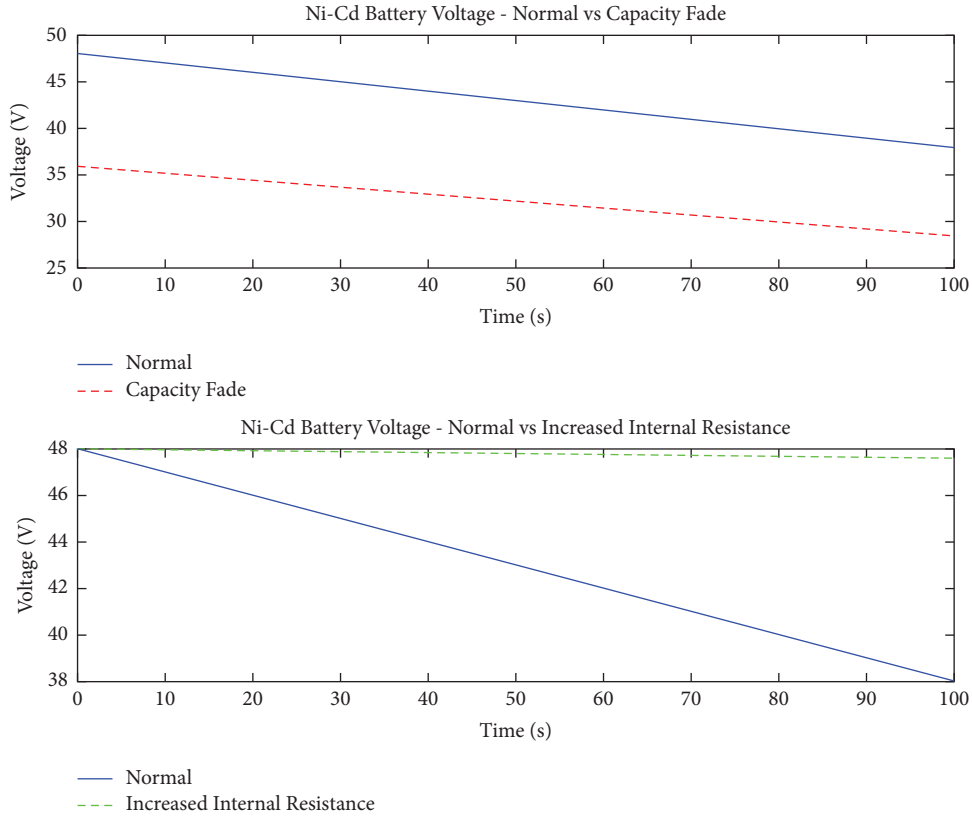

Figure 15: Ni-Cd battery voltage: normal vs. capacity fade.

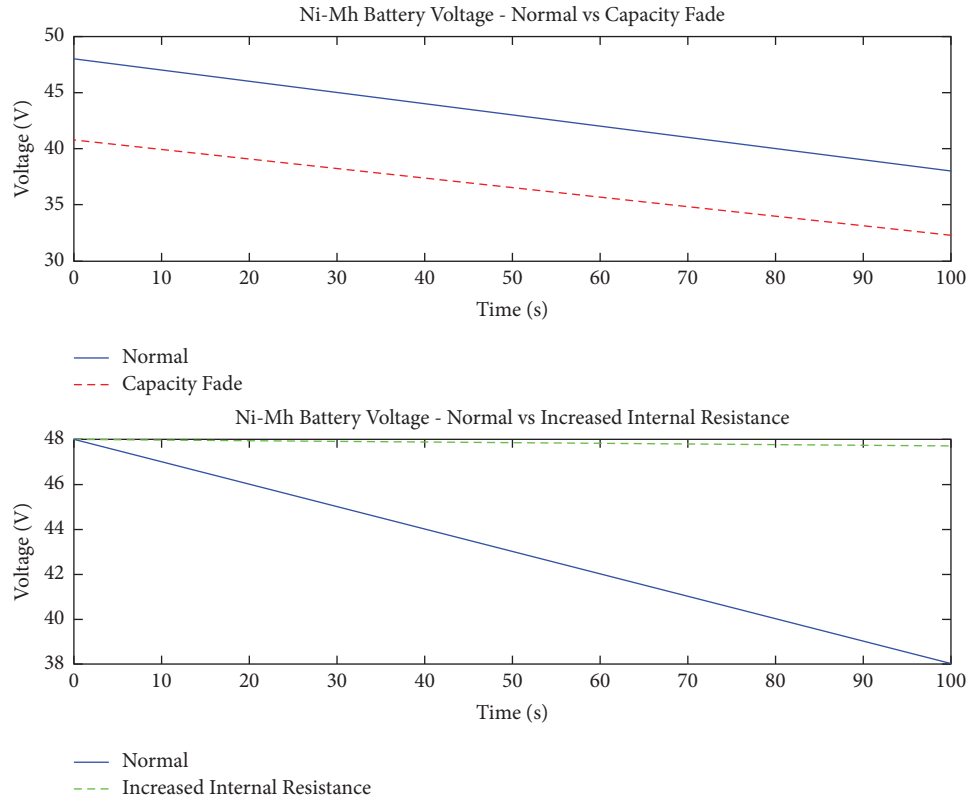

Figure 16: Ni-Mh battery voltage: normal vs. capacity fade.

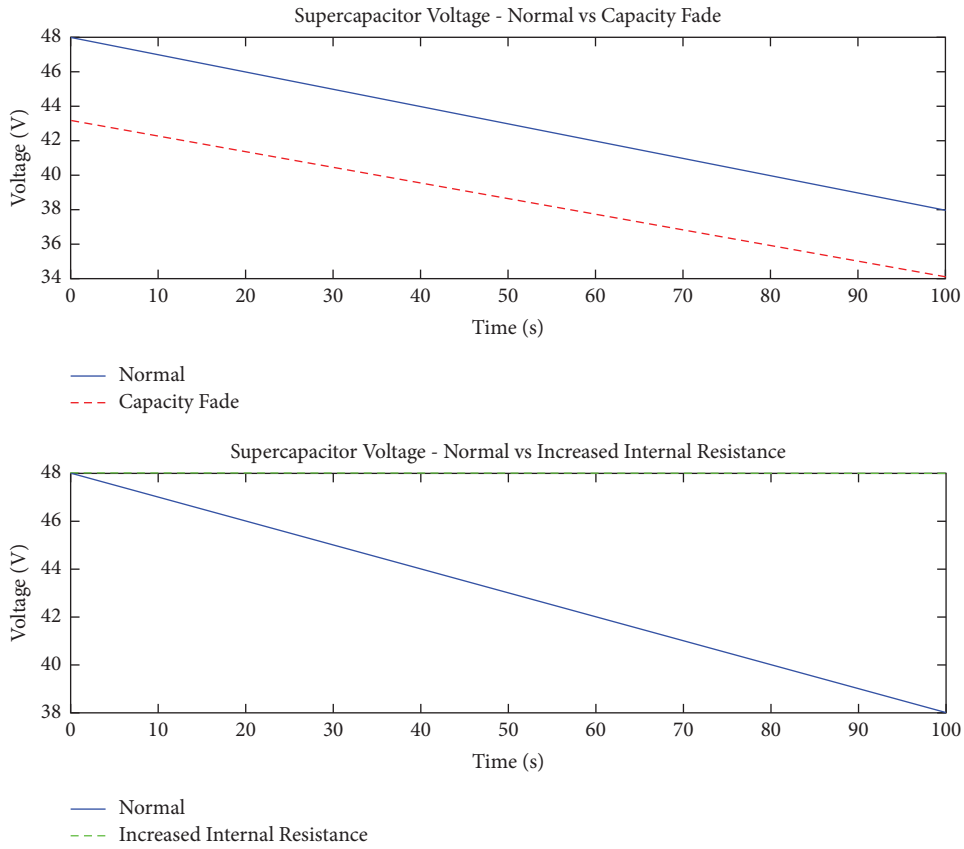

Figure 17: Supercapacitor voltage: normal vs. capacity fade.

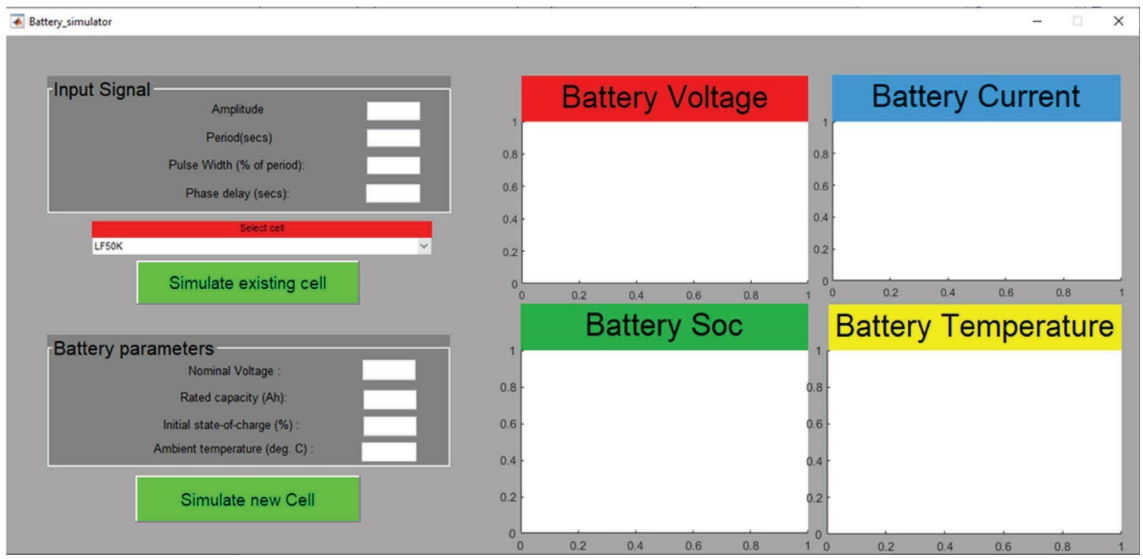

Figure 18: Simulator interface (GIU).

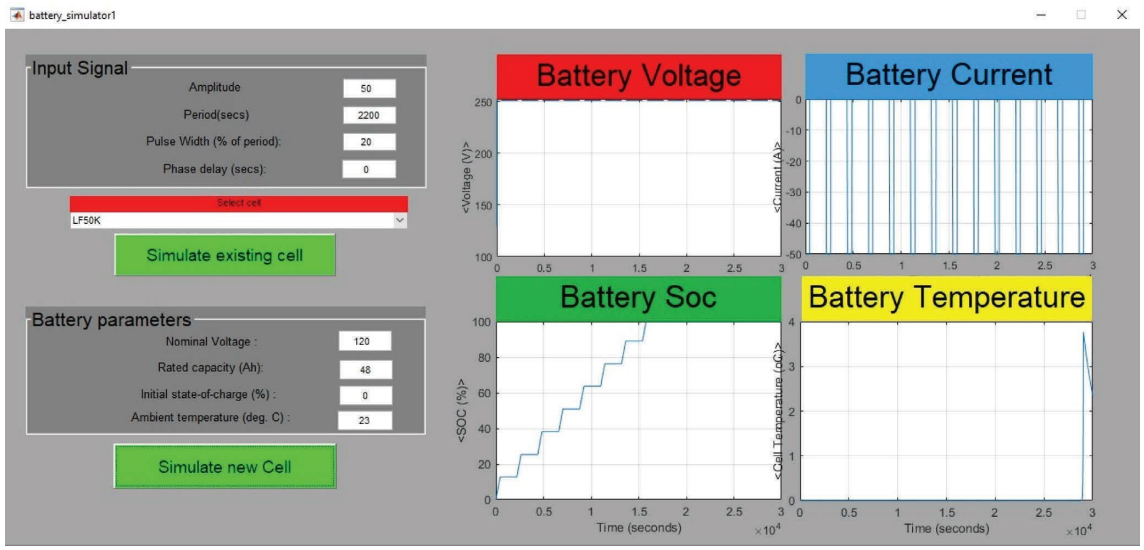

Figure 19: Charging parameters of the Li-ion battery (LFP).

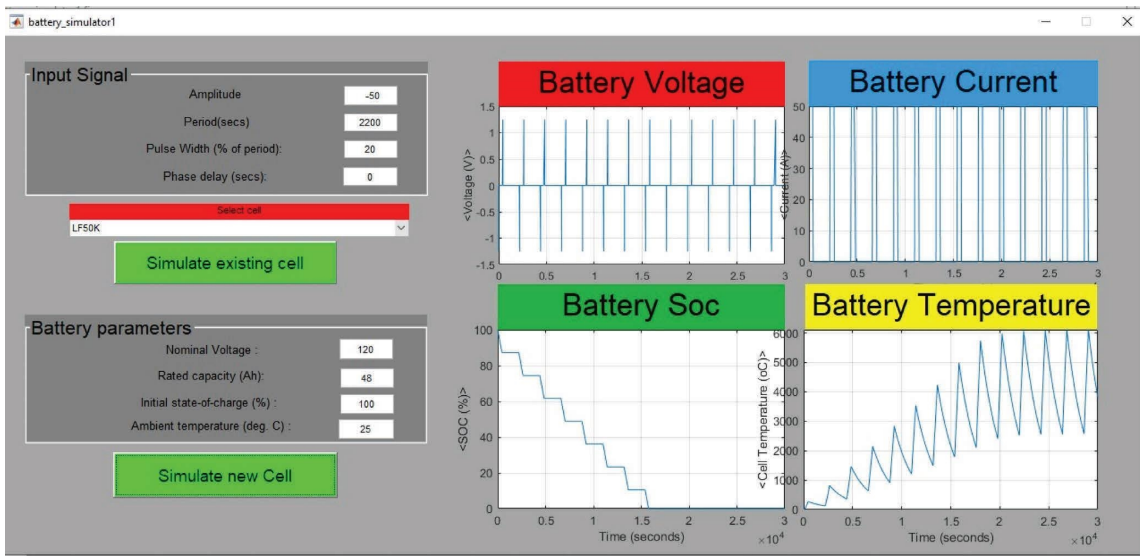

Figure 20: Li-ion battery discharging curve.

temperature of the battery cells. The results are described as follows:

(i) At $t = 0$ s, batteries A and B are discharged with 2 Amp at 80°C room temperature.

(ii) At $t = 150$ s, the inner temperature climbs to its steady-state value of 29.2°C due to the waste heat from the discharge operation. This causes a small rise in the output voltage of battery A, while the output voltage of battery B keeps falling.

(iii) At $t = 1000$ s, the surrounding temperature is reduced to −80°C. This leads to a sharp drop in the output voltage of battery A as the core temperature drops quickly. In addition, the SOC of the battery declines due to the reduction in its capacity. The output voltage of battery B continues to decrease at a slow rate until it reaches its equilibrium voltage.

(iv) At $t = 2000$ s, the surrounding temperature goes from −80°C to 0°C. As the core temperature builds up, the output voltage of battery A goes up. Similarly, as the capacity increases, the SOC of the battery grows. The output voltage of battery B remains constant until it reaches its equilibrium value.

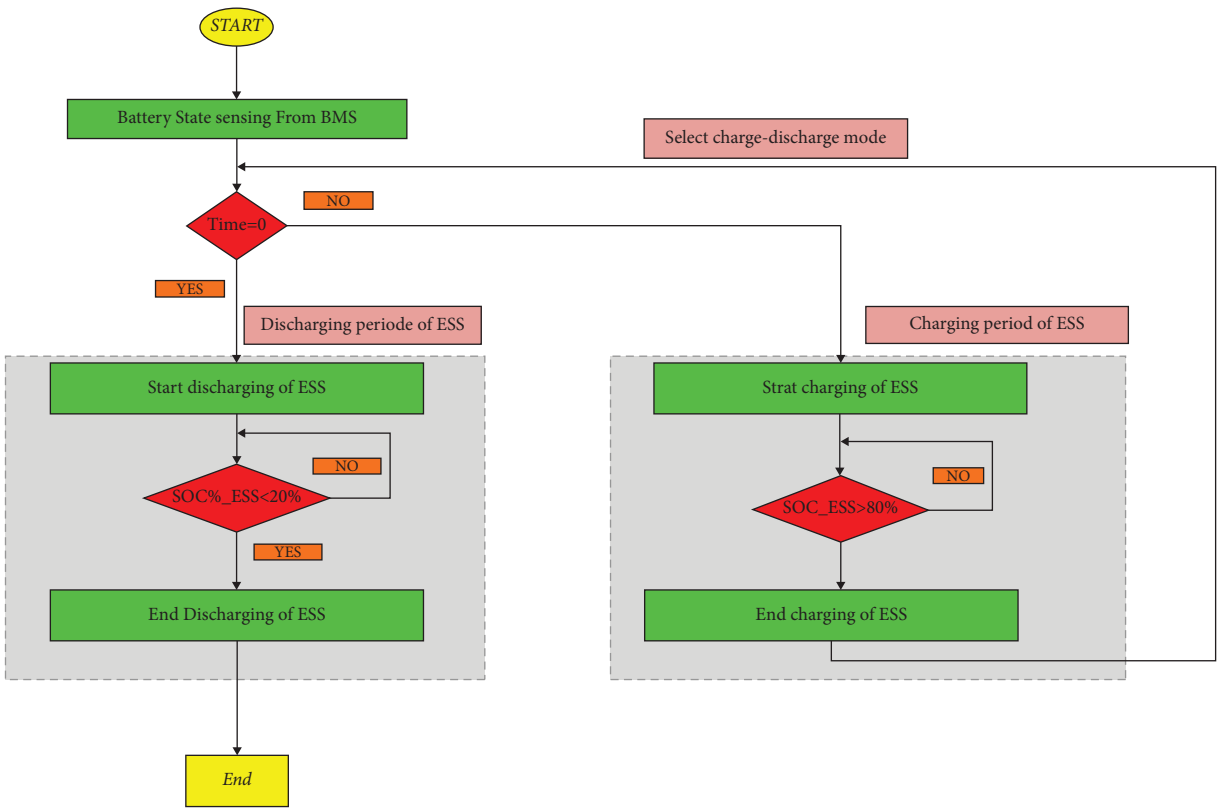

Figure 21: BMS charge/discharge optimization algorithm.

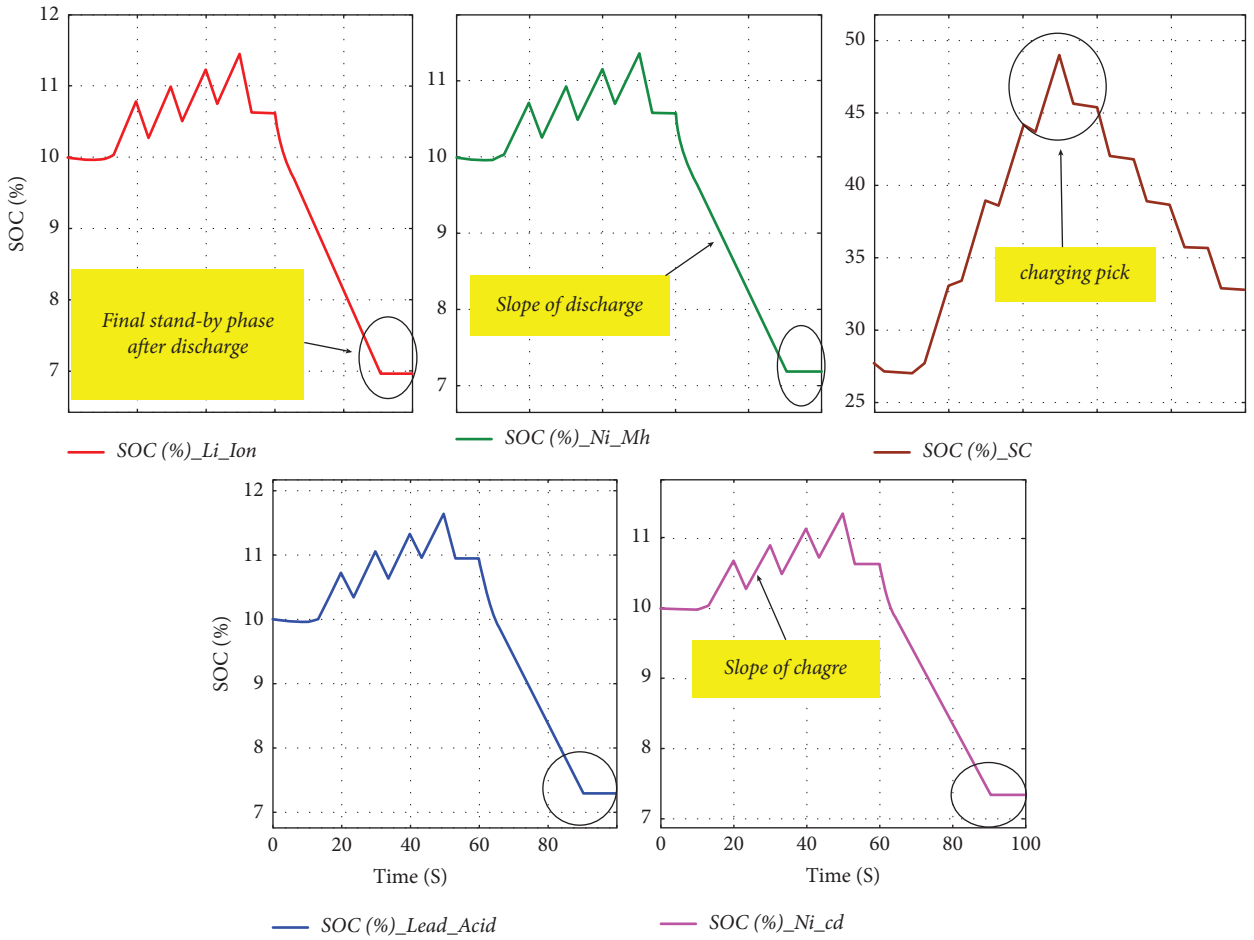

Figure 22: Charging/discharging curve of BESS managed by BMS.

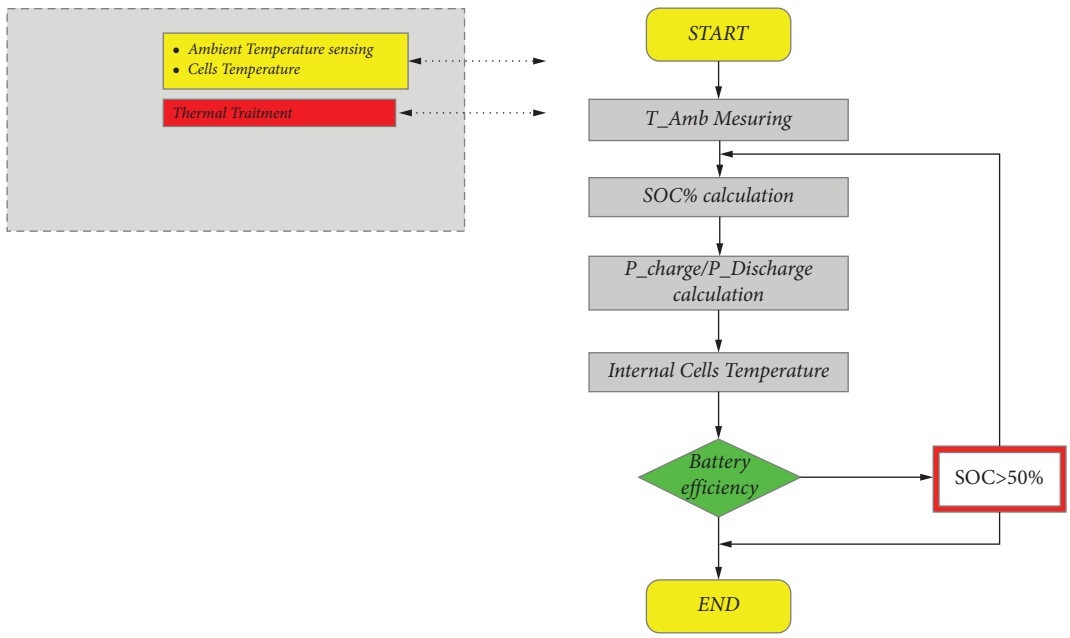

Figure 23: BMS algorithm considering ambient temperature.

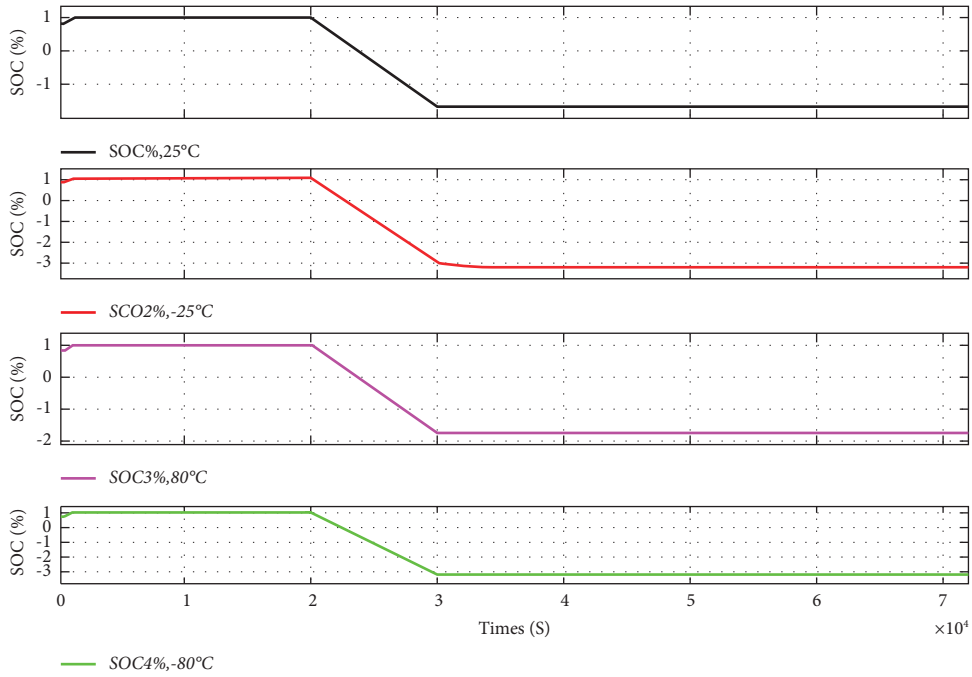

Figure 24: Variation in SOC as a function of ambient temperature.

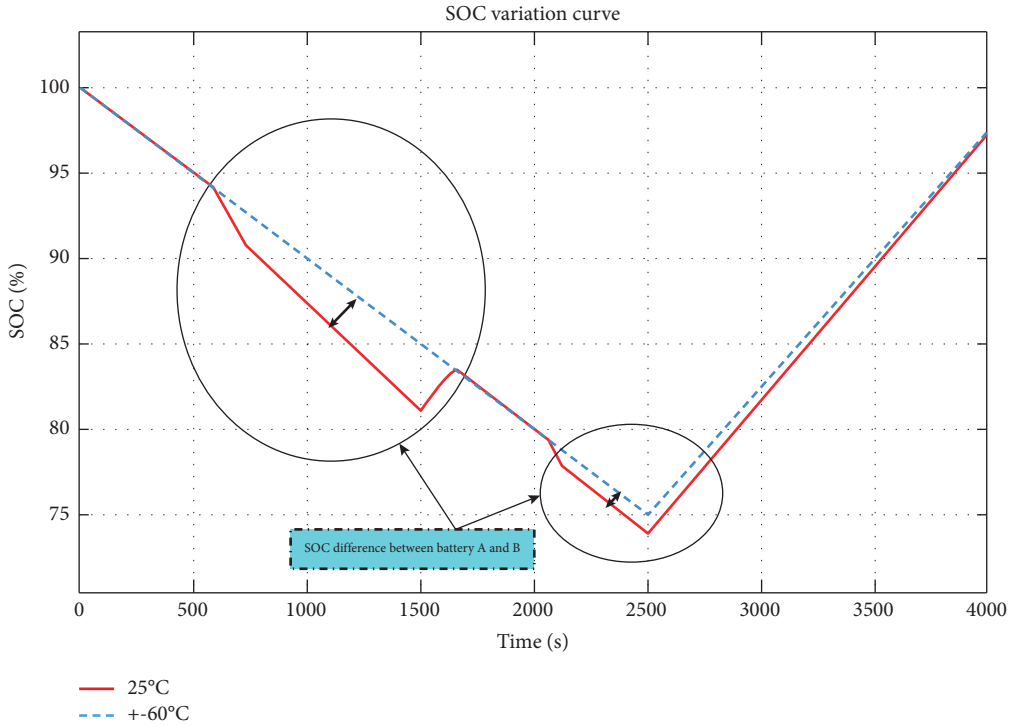

Figure 25: Comparison between the SOC of battery A and the SOC of battery B for case 1.

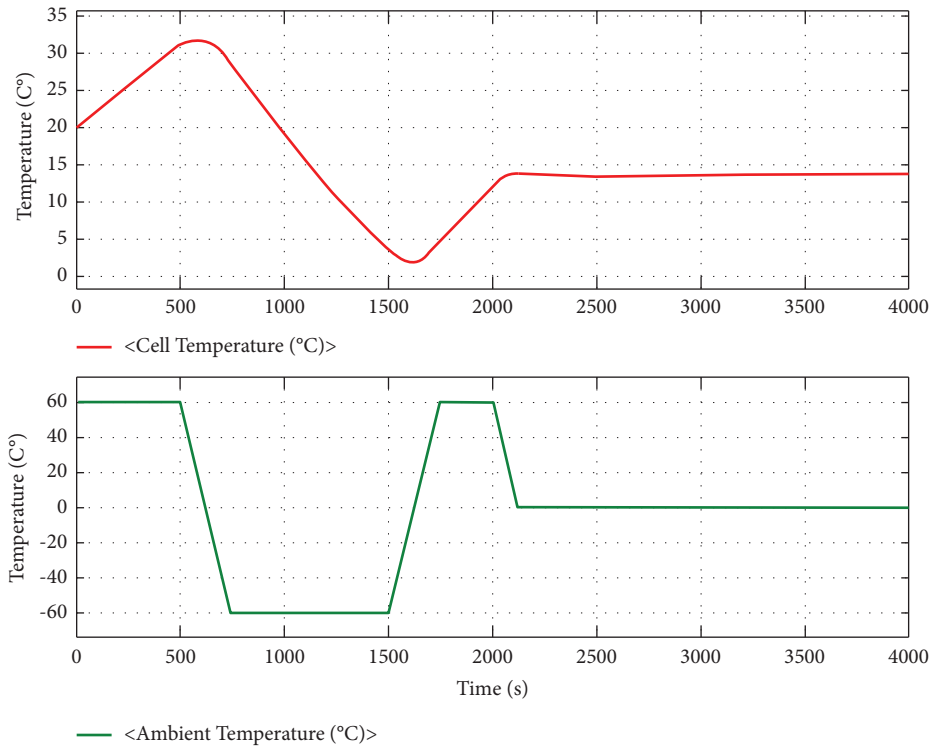

Figure 26: Internal and ambient temperature of battery A for case 1.

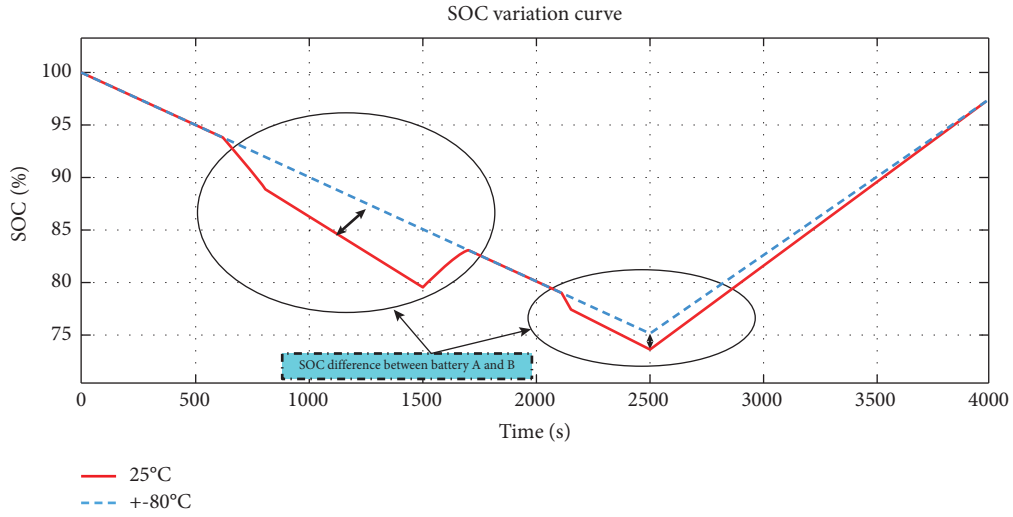

Figure 27: Comparison between the SOC of battery A and the SOC of battery B for case 2.

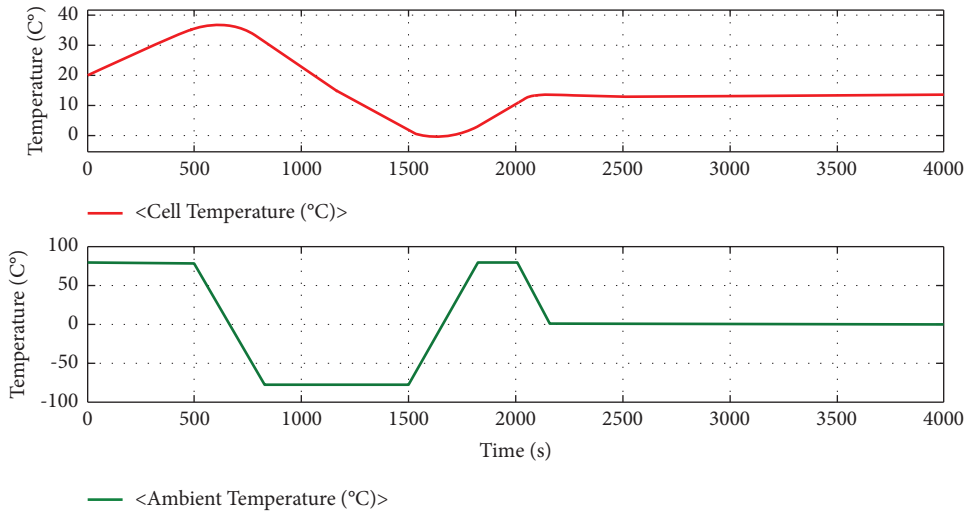

Figure 28: Internal and ambient temperature of battery A for case 2.

(v) At $t = 2500$ s, batteries A and B are charged with 3 Amp at an air temperature of 0°C. This leads to an increase in inner temperature due to the heat dissipation during the charging operation, which raises the charging voltage of battery A. Then, batteries A and B continue to charge until they are fully charged.

With the high level of temperature variation, the Li-ion battery loses its storage energy capacity, which can be seen between $t = 500$ s and $t = 1500$ s, where the curve varies from +60°C to −60°C. For the SOC of battery B (battery how influenced by temperature) in the discharge phase, battery B loses power more quickly than battery A (normal $T = 25$°C). When temperature increases from $t = 2500$ s to $t = 4000$ s (charging phase), battery B returns to gain its SOC, with all its performance. Even for SCs under the same test conditions on Simulink ($T = 25$°C, $T = 80$°C, $T = -25$°C, and $T = -80$°C), the ambient temperature has no effect whatsoever.

5. Conclusion

Different battery storage technologies for MGs have been analyzed and compared in this study. The development of an energy storage system for MGs is essential to ensure their successful functioning. This research has shown that the choice of a suitable combination of batteries and supercapacitors is highly dependent on the charging needs and the field of application of the MG. A combination of Li-ion batteries and SC offers high-energy density and a fast response time using the instantaneous response of SGs.

However, commercial factors and life span should also be considered when selecting a suitable ESS. Moreover, our research has highlighted the sensitivity of battery performance to ambient temperature changes. We have observed that most battery types, including Li-ion, lead-acid, and SCs, are affected by temperature variations, with an increase or decrease in storage capacity depending on the battery type. Therefore, optimizing the charging strategies of ESSs under different temperature conditions is an important research area that needs further investigation. In our future research, we will prioritize the integration of ESSs with renewable energy sources and explore MG optimization techniques to enhance the efficiency and reliability of MG systems. In addition, the development of new battery technologies with improved energy density, longer life span, and fast response time can enhance the performance of ESSs and MGs.

Nomenclature

I_{bat}: Battery current
I_{gas}: Gassing current
V_{bat}: Battery terminal voltage
V_{cc}: Internal battery voltage
SOC: Battery state of charge
SOC_0: Initial state of charge
A_{hd}: Ampere-hour discharged
R_i: Internal resistance
C_{dl}: Double-layer capacitance
A_{hd0}: Ampere-hour discharged at start of the process
Ah_{nom}: Nominal ampere-hour of battery
I_{mr}: Main reaction current in battery
SG: Battery-specific gravity
lSG_{full}: Specific density at full load
SG_{empty}: Full-load density
DK_{fit}: Parameter corresponding to discharge capacity of reference cell at an infinitesimal discharge current
R_{int}: Internal resistance
V_t: Terminal voltage
Q: Total capacity
$Z(t)$: State of charge at time t
E_{Nieq} and E_{Meq}: Equilibrium voltages
R_{Ni} and E_M: Connective resistances of nickel and metal
E_{Ni} and E_M: Battery energy
C_{dlNi} and E_{dlM}: Double-layer capacitors
R_e: Electrolyte resistance
$V(t)$: Voltage across the battery terminals at time t
V_{oc}: Open-circuit voltage of the battery at time t
$I(t)$: Current flowing through the battery at time t
R_0: Resistance of the charge-transfer reaction in the battery
R_1: Resistance of the diffusion process in the battery
C_0: Double-layer capacitance of the battery
C_1: Capacitance of the first RC branch
C_2: Capacitance of the second RC branch
$Q(t)$: Charge stored in the first RC branch at time t
$V_1(t)$: Voltage across the first RC branch at time t
$V_2(t)$: Voltage across the second RC branch at time t
$V_c(t)$: Voltage across the double-layer capacitance at time t.

Data Availability

The data used to support the findings of this study are included within the article.

Conflicts of Interest

The authors declare that they have no conflicts of interest.

Acknowledgments

The authors acknowledge "Researchers Supporting Project number (RSPD2023R685), King Saud University, Riyadh, Saudi Arabia."

References

[1] H. Wu, S. Wang, B. Zhao, and C. Zhu, "Energy management and control strategy of a grid-connected PV/battery system," *International Transactions on Electrical Energy Systems*, vol. 25, no. 8, pp. 1590–1602, 2015.

[2] R. Zieba Falama, F. D. Menga, M. Hamda Soulouknga, F. Kwefeu Mbakop, and C. Ben Salah, "A case study of an optimal detailed analysis of a standalone Photovoltaic/Battery system for electricity supply in rural and remote areas," *International Transactions on Electrical Energy Systems*, vol. 2022, Article ID 7132589, 12 pages, 2022.

[3] L. Frayssinet, "Heliatek: les films photovoltaïques, de la paillasse à l'usine," *The Journal of the Paris School of Management*, vol. 4, no. 6, pp. 30–36, 2019.

[4] J. K. Lundquist, K. K. Duvivier, D. Kaffine, and J. M. Tomaszewski, "Costs and consequences of wind turbine wake effects arising from uncoordinated wind energy development," *Nature Energy*, vol. 4, no. 1, pp. 26–34, 2018.

[5] A. Gloe, C. Jauch, and T. Räther, "Grid support with wind turbines: the case of the 2019 blackout in Flensburg," *Energies*, vol. 14, no. 6, p. 1697, 2021.

[6] D. Perez-DeLaMora, J. E. Quiroz-Ibarra, G. Fernandez-Anaya, and E. Hernandez-Martinez, "Roadmap on community-based microgrids deployment: an extensive review," *Energy Reports*, vol. 7, pp. 2883–2898, 2021.

[7] A. Farjah, T. Ghanbari, and A. R. Seifi, "Contribution management of lead-acid battery, Li-ion battery, and supercapacitor to handle different functions in EVs," *International Transactions on Electrical Energy Systems*, vol. 30, no. 1, 2019.

[8] R. Raj Shrivastwa, H. Ahmad, K. Melizi, and S. Bacha, "Understanding microgrids and their future trends," in *Proceedings of the IEEE International Conference on Industrial Technology (ICIT)*, Melbourne, Australia, February 2019.

[9] A. Z. Al Shaqsi, K. Sopian, and A. Al-Hinai, "Review of energy storage services, applications, limitations, and benefits," *Energy Reports*, vol. 6, pp. 288–306, 2020.

[10] J. J. Hargreaves and R. A. Jones, "Long term energy storage in highly renewable systems," *Frontiers in Energy Research*, vol. 8, p. 219, 2020.

[11] N. A. Sepulveda, J. D. Jenkins, A. Edington, D. S. Mallapragada, and R. K. Lester, "The design space for long-duration energy storage in decarbonized power systems," *Nature Energy*, vol. 6, no. 5, pp. 506–516, 2021.

[12] T. V. Muni and S. V. N. L. Lalitha, "Fast acting mppt controller for solar pv with energy management for dc microgrid," *International Journal of Engineering and Advanced Technology*, vol. 8, 2019.

[13] U. R. H. Habib, S. Wang, and M. T. Aziz, "PV-wind-battery based standalone microgrid system with MPPT for green and sustainable future," in *Proceedings of the IEEE 9th International Conference on Power and Energy Systems (ICPES)*, pp. 10–12, Perth, Australia, December 2019.

[14] V. Subramanian, V. Indragandhi, R. Kuppusamy, and Y. Teekaraman, "Modeling and analysis of PV system with fuzzy logic MPPT technique for a DC microgrid under variable atmospheric conditions," *Electronics*, vol. 10, no. 20, p. 2541, 2021.

[15] X. Hu, S. Li, and H. Peng, "A comparative study of equivalent circuit models for Li-ion batteries," *Journal of Power Sources*, vol. 198, pp. 359–367, 2012.

[16] M.-K. Tran, A. DaCosta, A. Mevawalla, S. Panchal, and M. Fowler, "Comparative study of equivalent circuit models performance in four common lithium-ion batteries: lfp, nmc, lmo, NCA," *Batteries*, vol. 7, no. 3, p. 51, 2021.

[17] S. Z. Zhang and X. W. Zhang, "A comparative study of different online model parameters identification methods for lithium-ion battery," *Science China Technological Sciences*, vol. 64, no. 10, pp. 2312–2327, 2021.

[18] P. Dost and C. Sourkounis, "Generalized lead-acid based battery model used for a battery management system," *Athens Journal of Technology & Engineering*, vol. 3, pp. 255–270, 2016.

[19] L. El Mehdi, E. F. Anas, M. Zazi, and E. B. Abdessamad, "Comparative study of lead acid battery modelling," *ARPN Journal of Engineering and Applied Sciences*, vol. 13, pp. 4448–4452, 2018.

[20] H. Rami, A. El-Shahat, and K. Youakim, "Lead acid battery modeling for PV applications," *Journal of Electrical Engineering*, vol. 15, no. 2, p. 17, 2015.

[21] S. S. Giuliano, C. L. Nascimento, and J. A. Geraldo, "Modeling and simulation of nickel-cadmium batteries during discharge," in *Proceedings of the IEEE Aerospace Conference*, pp. 5–12, Big Sky, MT, USA, March 2011.

[22] J. O. Oladigbolu, Y. A. Al-Turki, and L. Olatomiwa, "Comparative study and sensitivity analysis of a standalone hybrid energy system for electrification of rural healthcare facility in Nigeria," *Alexandria Engineering Journal*, vol. 60, no. 6, pp. 5547–5565, 2021.

[23] S. Reddy Salkuti and C. Mook Jung, "Comparative analysis of storage techniques for a grid with renewable energy sources," *International Journal of Engineering & Technology*, vol. 7, no. 3, pp. 970–976, 2018.

[24] P. Nikolaidis and A. Poullikkas, "A comparative review of electrical energy storage systems for better sustainability," *Journal of power technologies*, vol. 97, no. 3, pp. 220–245, 2017.

[25] M. Moncecchi, C. Brivio, S. Mandelli, and M. Merlo, "Battery energy storage systems in microgrids: modeling and design criteria," *Energies*, vol. 13, no. 8, p. 2006, 2020.

[26] C. Deepak and M. Anwar, "Microgrid battery energy storage systems (BESS) approach," *Journal of Advanced Research in Power Electronics & Power Systems*, vol. 5, no. 1, pp. 15–18, 2018.

[27] J. Hernández, A. F. Campos, and R. Gómez, "State of charge and state of health determination model for a lead-acid battery to be implemented in a management system," *WIT Transactions on Ecology and the Environment*, vol. 195, pp. 243–255, 2015.

[28] J. Badeda, M. Huck, D. U. Sauer, J. Kabzinski, and J. Wirth, "Basics of lead–acid battery modelling and simulation," *Lead-acid batteries for future automobiles*, pp. 463–507, 2017.

[29] L. Devarakonda and T. Hu, "Effects of rest time on discharge response and equivalent circuit model for a lead-acid battery," *Journal of Power Sources*, vol. 282, pp. 19–27, 2015.

[30] J. Lee, J. M. Kim, J. Yi, and C. Y. Won, "Battery management system algorithm for energy storage systems considering battery efficiency," *Electronics*, vol. 10, no. 15, p. 1859, 2021.

[31] A. Selmani, A. Ed-Dahhak, M. Outanoute, A. Lachhab, M. Guerbaoui, and B. Bouchikhi, "Performance evaluation of modelling and simulation of lead acid batteries for photovoltaic applications," *International Journal of Power Electronics and Drive Systems*, vol. 7, no. 2, p. 472, 2016.

[32] C. Chang, Y. Zheng, and Y. Yu, "Estimation for battery state of charge based on temperature effect and fractional extended kalman filter," *Energies*, vol. 13, no. 22, p. 5947, 2020.

[33] J. Loukil, F. Masmoudi, and N. Derbel, "A real-time estimator for model parameters and state of charge of lead acid batteries in photovoltaic applications," *Journal of Energy Storage*, vol. 34, Article ID 102184, 2021.

[34] J. Han, D. Kim, and M. Sunwoo, "State-of-charge estimation of lead-acid batteries using an adaptive extended Kalman filter," *Journal of Power Sources*, vol. 188, no. 2, pp. 606–612, 2009.

[35] C. Ge, Y. Zheng, and Y. Yu, "State of charge estimation of lithium-ion battery based on improved forgetting factor recursive least squares-extended Kalman filter joint algorithm," *Journal of Energy Storage*, vol. 55, Article ID 105474, 2022.

[36] M.-K. Tran, A. Mevawala, S. Panchal, K. Raahemifar, M. Fowler, and R. Fraser, "Effect of integrating the hysteresis component to the equivalent circuit model of Lithium-ion battery for dynamic and non-dynamic applications," *Journal of Energy Storage*, vol. 32, Article ID 101785, 2020.

[37] D. Elena, L. Dorin Dumitru, and L. Gheorghe, "Models and modelling the supercapacitors for a defined application," *Annals of the University of Craiova, Electrical Engineering series*, vol. 35, pp. 200–205, 2011.

[38] D. Xu, L. Zhang, B. Wang, and G. Ma, "A novel equivalent-circuit model and parameter identification method for supercapacitor performance," *Energy Procedia*, vol. 145, pp. 133–138, 2018.

[39] N. Ma, D. Yang, S. Riaz, L. Wang, and K. Wang, "Aging mechanism and models of supercapacitors: a review," *Technologies*, vol. 11, no. 2, p. 38, 2023.

[40] W. Mitkowski and P. Skruch, "Fractional-order models of the supercapacitors in the form of RC ladder networks," *Bulletin of the Polish Academy of Sciences, Technical Sciences*, vol. 61, no. 3, pp. 581–587, 2013.

[41] N. El Ghossein, J. P. Salameh, N. Karami, M. El Hassan, and M. B. Najjar, "Survey on electrical modeling methods applied on different battery types," in *Proceedings of the IEEE Third International Conference on Technological Advances in Electrical, Electronics and Computer Engineering (TAEECE)*, Beirut, Lebanon, May 2015.

[42] M. B. A. Zahran and A. Atef, "Electrical and thermal properties of nicd battery for low earth orbit satellite's applications," *WSEAS Transactions on Electronics*, vol. 3, no. 6, p. 340, 2006.

[43] S. Fang, Y. Xu, Z. Li, T. Zhao, and H. Wang, "Two-step multi-objective management of hybrid energy storage system in all-electric ship microgrids," *IEEE Transactions on Vehicular Technology*, vol. 68, no. 4, pp. 3361–3373, 2019.

[44] K. Liu, K. Li, Q. Peng, and C. Zhang, "A brief review on key technologies in the battery management system of electric vehicles," *Frontiers of Mechanical Engineering*, vol. 14, no. 1, pp. 47–64, 2019.

[45] N. G. Panwar, S. Singh, A. Garg, A. K. Gupta, and L. Gao, "Recent advancements in battery management system for Li-ion batteries of electric vehicles: future role of digital twin, cyber-physical systems, battery swapping technology, and nondestructive testing," *Energy Technology*, vol. 9, no. 8, Article ID 2000984, 2021.

[46] B. Zou, L. Zhang, X. Xue et al., "A review on the fault and defect diagnosis of lithium-ion battery for electric vehicles," *Energies*, vol. 16, no. 14, 2023.

[47] X. Hu, K. Zhang, K. Liu, X. Lin, S. Dey, and S. Onori, "Advanced Fault diagnosis for lithium-ion battery systems: a review of fault mechanisms, fault features, and diagnosis procedures," *IEEE Industrial Electronics Magazine*, vol. 14, no. 3, pp. 65–91, 2020.

[48] L. Yao, S. Xu, A. Tang et al., "A review of lithium-ion battery state of health estimation and prediction methods," *World Electric Vehicle Journal*, vol. 12, no. 3, 2021.

[49] J. Jiang, T. Li, C. Chang, C. Yang, and L. Liao, "Fault diagnosis method for lithium-ion batteries in electric vehicles based on isolated forest algorithm," *Journal of Energy Storage*, vol. 50, Article ID 104177, 2022.

[50] S. Jiang and Z. Song, "A review on the state of health estimation methods of lead-acid batteries," *Journal of Power Sources*, vol. 517, Article ID 230710, 2022.

[51] I. B. Espedal, A. Jinasena, O. S. Burheim, and J. J. Lamb, "Current trends for state-of-charge (SoC) estimation in lithium-ion battery electric vehicles," *Energies*, vol. 14, no. 11, 2021.

[52] N. Xu, Y. Xie, Q. Liu, F. Yue, and D. Zhao, "A data-driven approach to state of health estimation and prediction for a lithium-ion battery pack of electric buses based on real-world data," *Sensors*, vol. 22, no. 15, 2022.

[53] J. Zhang and C. Xia, "State-of-charge estimation of valve regulated lead acid battery based on multi-state Unscented Kalman Filter," *International Journal of Electrical Power & Energy Systems*, vol. 33, no. 3, pp. 472–476, 2011.

[54] J. D. Velásquez, L. Cadavid, and C. J. Franco, "Intelligence techniques in sustainable energy: analysis of a decade of advances," *Energies*, vol. 16, no. 19, 2023.

[55] B. Liu, Y. Xu, H. Zhang et al., "State of charge estimation of supercapacitor under different temperatures using particle filter algorithm based on fractional-order model," *Journal of the Electrochemical Society*, vol. 170, no. 9, Article ID 090541, 2023.

[56] A. Mejdoubi, H. Chaoui, H. Gualous, A. Oukaour, Y. Slamani, and J. Sabor, "Supercapacitors state-of-health diagnosis for electric vehicle applications," *World Electric Vehicle Journal*, vol. 8, no. 2, pp. 379–387, 2016.

[57] N. Noura, L. Boulon, and S. Jemeï, "A review of battery state of health estimation methods: hybrid electric vehicle challenges," *World Electric Vehicle Journal*, vol. 11, no. 4, 2020.

[58] K. Yang, L. Zhang, Z. Zhang et al., "Battery state of health estimate strategies: from data analysis to end-cloud collaborative framework," *Batteries*, vol. 9, no. 7, p. 351, 2023.

[59] Z. Sun, Z. Wang, P. Liu et al., "An online data-driven fault diagnosis and thermal runaway early warning for electric vehicle batteries," *IEEE Transactions on Power Electronics*, vol. 37, no. 10, pp. 12636–12646, 2022.

[60] A. J. Telmoudi, M. Soltani, Y. Ben Belgacem, and A. Chaari, "Modeling and state of health estimation of nickel–metal hydride battery using an EPSO-based fuzzy c-regression model," *Soft Computing*, vol. 24, no. 10, pp. 7265–7279, 2020.

[61] J. B. Sangiri, T. Kulshreshtha, S. Ghosh, S. Maiti, and C. Chakraborty, "A novel methodology to estimate the state-of-health and remaining-useful-life of a Li-ion battery using discrete Fourier transformation," *Journal of Energy Storage*, vol. 46, Article ID 103849, 2022.

[62] A. Tomaszewska, Z. Chu, X. Feng et al., "Lithium-ion battery fast charging: a review," *eTransportation*, vol. 1, Article ID 100011, 2019.

[63] M. Al-Saadi, J. Olmos, A. Saez-de-Ibarra, J. Van Mierlo, and M. Berecibar, "Fast charging impact on the lithium-ion batteries' lifetime and cost-effective battery sizing in heavy-duty electric vehicles applications," *Energies*, vol. 15, no. 4, 2022.

[64] Math Works, "Lithium-ion temperature dependent battery model," 2023, https://uk.mathworks.com/help/sps/ug/lithium-ion-temperature-dependent-battery-model.html.